Marine Geology 443 (2022) 106674

Contents lists available at ScienceDirect

Marine Geology

journal homepage: www.elsevier.com/locate/margo

Pleistocene depositional environments and links to cryosphere-ocean interactions on the eastern Ross Sea continental slope, Antarctica (IODP Hole U1525A)

Maxine V. King [a,*], Jenny A. Gales [a], Jan Sverre Laberg [b], Robert M. McKay [c], Laura De Santis [d], Denise K. Kulhanek [e], Phil J. Hosegood [a], Antony Morris [f], IODP Expedition 374 Scientists[g]

[a] School of Marine and Biological Sciences, University of Plymouth, Drake Circus, Plymouth PL4 8AA, UK
[b] Department of Geosciences, UIT The Arctic University of Norway, Postboks 6050 Langnes, N-9037 Tromsø, Norway
[c] Antarctic Research Centre, Victoria University of Wellington, PO Box 600, Wellington 6140, New Zealand
[d] National Institute of Oceanography and Applied Geophysics (OGS), Borgo Grotta Gigante, 42/c, 34010 Sgonico, TS, Italy
[e] Institute of Geosciences, Christian-Albrechts-University of Kiel, Ludewig-Meyn-Straße 14, 24118 Kiel, Germany
[f] School of Geography, Earth and Environmental Sciences, University of Plymouth, Drake Circus, Plymouth PL4 8AA, UK
[g] International Ocean Discovery Program, Texas A&M University, 1000 Discovery Drive, College Station, TX 77845, USA

ARTICLE INFO

Editor: Michele Rebesco

Keywords:
Eastern Ross Sea
Sedimentary process
Trough-mouth fan
Turbidites
Pleistocene

ABSTRACT

The repeated proximity of West Antarctic Ice Sheet (WAIS) ice to the eastern Ross Sea continental shelf break during past ice age cycles has been inferred to directly influence sedimentary processes occurring on the continental slope, such as turbidity current and debris flow activity; thus, the records of these processes can be used to study the past history of the WAIS. Ross Sea slope sediments may additionally provide an archive on the history and interplay of density-driven or geostrophic oceanic bottom currents with ice-sheet-driven depositional mechanisms. We investigate the upper 121 m of Hole U1525A, collected during International Ocean Discovery Program (IODP) Expedition 374 in 2018. Hole U1525A is located on the southwestern external levee of the Hillary Canyon (Ross Sea, Antarctica) and the depositional lobe of the nearby trough-mouth fan. Using core descriptions, grain size analysis, and physical properties datasets, we develop a lithofacies scheme that allows construction of a detailed depositional model and environmental history of past ice sheet-ocean interactions at the eastern Ross Sea continental shelf break/slope since ~2.4 Ma. The earliest Pleistocene interval (~2.4- ~ 1.4 Ma) represents a hemipelagic environment dominated by ice-rafting and reworking/deposition by relatively persistent bottom current activity. Finely interlaminated silty muds with ice-rafted debris (IRD) layers are interpreted as contourites. Between ~1.4 and ~0.8 Ma, geostrophic bottom current activity was weaker and turbiditic processes more common, likely related to the increased proximity of grounded ice at the shelf edge. Silty, normally-graded laminations with sharp bases may be the result of flow-stripped turbidity currents overbanking the canyon levee during periods when ice was grounded at or proximal to the shelf edge. A sandy, IRD- and foraminifera-bearing interval dated to ~1.18 Ma potentially reflects warmer oceanographic conditions and a period of stronger Antarctic Slope Current flow. This may have enhanced upwelling of warm Circumpolar Deep Water onto the shelf, leading to large-scale glacial retreat at that time. The thickest interval of turbidite interlamination was deposited after ~1 Ma, following the onset of the Mid-Pleistocene Transition, interpreted as a time when most ice sheets grew and glacial periods were longer and more extreme. Sedimentation after ~0.8 Ma was dominated by glacigenic debris flow deposition, as the trough mouth fan that dominates the eastern Ross Sea continental slope prograded and expanded over the site. These findings will help to improve estimations of WAIS ice extent in future Ross Sea shelf-based modelling studies, and provide a basis for more detailed analysis of the inception and growth of the WAIS under distinct oceanographic conditions.

* Corresponding author at: School of Marine and Biological Sciences, Marine Building, University of Plymouth, James Street, Plymouth, Devon PL4 6EQ, UK.
E-mail addresses: E-mail addresses: maxine.king@plymouth.ac.uk (M.V. King), jenny.gales@plymouth.ac.uk (J.A. Gales), jan.laberg@uit.no (J.S. Laberg), robert.mckay@vuw.ac.nz (R.M. McKay), ldesantis@inogs.it (L. De Santis), denise.kulhanek@ifg.uni-kiel.de (D.K. Kulhanek), phil.hosegood@plymouth.ac.uk (P.J. Hosegood), antony.morris@plymouth.ac.uk (A. Morris). Expedition_374_Participants@iodp.tamu.edu ().

https://doi.org/10.1016/j.margeo.2021.106674
Received 13 May 2021; Received in revised form 7 October 2021; Accepted 14 October 2021
Available online 22 October 2021
0025-3227/© 2021 Elsevier B.V. All rights reserved.

1. Introduction

Recent accelerated rates of ice mass loss from the West Antarctic Ice Sheet (WAIS), driven by enhanced oceanic-induced melting, have demonstrated the urgent need for a refined understanding of past ocean-ice sheet interactions on the Antarctic margin (Harig and Simons, 2015; Shepherd et al., 2018; Rignot et al., 2019). The WAIS is generally grounded well below sea level on overdeepened continental shelves, contributing towards an unstable ice sheet that is highly responsive to oceanic and atmospheric variability (Hughes, 1973; Schröder et al., 2019). Recent studies show that the average WAIS thinning rate continues to increase and has provided the largest contribution to overall mass loss of the Antarctic Ice Sheet (AIS) since 2000 (McMillan et al., 2014; Shepherd et al., 2018). The rapid nature of these losses is reflected in rising sea level and changing global climate (Dangendorf et al., 2019). Furthermore, modern estimates predict oceanic-induced basal melting removes approximately half of all gains in AIS surface mass before reaching the calving zone of an ice shelf (Depoorter et al., 2013). This emphasises the need for improved constraints on past grounded ice and oceanographic variability during periods of ice sheet growth and retreat.

The Ross Sea has been the subject of extensive studies to explore its glacial history, sedimentary environments, and oceanographic regimes; particularly through large-scale ventures such as ANTOSTRAT (Antarctic Offshore Stratigraphy Project) and ANDRILL (Antarctic Drilling Project) (ANTOSTRAT, 1995; Naish et al., 2009; Mckay et al., 2012). However, until recently, such studies have primarily focused on collecting data from the mid continental shelf, where sequences provide direct records of ice sheet advance but preserve a highly discontinuous record due to glacial overriding. Consequently, investigating the sedimentary mechanisms operating on the Ross Sea continental slope over time can help to decode regional oceanographic change, and also provide a valuable stratigraphic connection to discontinuous shelf records of ice shelf variability that are subject to the erosive action of grounded ice (Barker et al., 1999; Barker and Camerlenghi, 2002; Rebesco et al., 2006). Interpretation of sedimentary sequences from this region of the Antarctic continental margin may also help to understand complex interactions between along- and down-slope processes, which are further complicated by Coriolis-driven offset (Kuvaas et al., 2005; Rebesco et al., 2007; Salles et al., 2010; Alonso et al., 2016; Miramontes et al., 2020).

We use sediments collected during International Ocean Discovery Program (IODP) Expedition 374 to provide a detailed description of the depositional environment on the eastern Ross Sea continental slope during the Pleistocene. This will help to improve interpretations of grounded ice activity on the continental shelf, and investigate changes in regional-scale oceanographic features (e.g. downslope flow of dense water from sea ice production on the shelf; along-slope flow of bottom currents) that may be linked to changing ice cover on the continental shelf. Using these data, we aim to understand: 1) the processes that operated on the eastern Ross Sea upper slope, Antarctica, during the Pleistocene; 2) the characteristics, timing and frequency of these processes and 3) how they relate to glacial/interglacial cycles. The palaeo-sedimentary signature of these processes may reveal important information regarding regional palaeo-ice sheet dynamics and the wider behaviour of the WAIS in response to climate forcing.

1.1. Regional setting

IODP Site U1525 was drilled in 2018 and is located on the upper continental slope in the eastern Ross Sea, Antarctica, ~60 km northeast of the continental shelf break at 1776 m water depth (75°0.06′S, 173°55.20′W; Fig. 1) (McKay et al., 2019b). Site U1525 lies on the gently-sloping flank of an asymmetric sediment mound on the continental slope that forms part of the southwestern external levee of the Hillary Canyon, to the southeast of the Iselin Bank (McKay et al., 2019b).

In the eastern Ross Sea, ice drains through fast ice streams from the WAIS, calving at the modern-day ice front of the Ross Ice Shelf roughly 350-375 km landward from the continental shelf break (Anderson et al., 1984; Bart, 2004). Along this section of the margin, the Glomar Challenger and Pennell Troughs bisect the shelf break, which are thought to be the location of palaeo-ice streams during past glacial periods (Cooper et al., 1991; De Santis et al., 1995; Shipp et al., 1999). Deeply-incised gully and channel systems are potentially related to canyon head processes in the Hillary Canyon (Gales et al., 2021). A prograding trough-mouth fan (TMF) system lies to the east of the canyon (Fig. 1a–b and Fig. F24 in McKay et al., 2019b) (Alonso et al., 1992). High input of glacigenic sediments through these troughs during glacial periods were likely responsible for the formation of this fan.

A number of seismic and sedimentological studies conducted in the Ross Sea have revealed several periods of glacial advance and retreat over the Pleistocene, including instances where WAIS ice was grounded at the continental shelf break during pronounced glacial periods such as the last glacial maximum (LGM) (Anderson et al., 1984; De Santis et al., 1999; Bart, 2004; Mosola and Anderson, 2006; Bart and Owolana, 2012; Halberstadt et al., 2016; Prothro et al., 2018). Strong seismic reflectors, known as the Ross Sea seismic unconformities (RSU1–6), record the major ice sheet grounding events since the Oligocene (RSU6; ~30 Ma) (De Santis et al., 1999). An R/V OGS Explora cruise funded by the Antarctic Italian Program "Programma Nazionale delle Ricerche in Antartide" collected seismic reflection data in 1994 from across Site U1525 (Fig. 1c), which showed the presence of such reflectors on the slope that have been interpreted as RSU2–4 (4–2.5 Ma, 10–5.5 Ma and ~ 15.8–14.6 Ma respectively) (Brancolini et al., 1995; McKay et al., 2019b; Conte et al., 2021). These data also show a ~ 1 km-thick sequence of mostly high to medium amplitude, parallel and internally stratified reflectors indicative of sediment drifts, and the overspill and flow-stripping deposits of turbidity currents on the slope. The uppermost seismic unit of the TMF shows acoustically-transparent or chaotic deposits consistent with glacigenic debris flows above RSU2, burying sediment drifts and channel-levees in the continental slope (Fig. 1c), and suggesting major progradation of the fan during the late Pliocene/early Pleistocene (4.0–2.5 Ma) in response to changing glacial dynamics (Lindeque et al., 2016; Kim et al., 2018; Conte et al., 2021). Volumetric-based assessments of grounding-zone wedges in the Glomar Challenger Trough suggest grounding line advance over the last glacial cycle may have been as rapid as 13 m/yr; although this value is not a precise measure, it illustrates the potential for dynamic WAIS behaviour in the Ross Sea (Bart and Owolana, 2012).

Oceanographically, the Hillary Canyon is a significant location in the Ross Sea for dense shelf water overflow into the deep ocean, which mixes with Modified Circumpolar Deep Water to form Antarctic Bottom Water (Bergamasco et al., 2002; Budillon et al., 2002; Whitworth and Orsi, 2006; Budillon et al., 2011). Down-slope flows of dense shelf water are deflected westward due to the Coriolis force (Morrison et al., 2020). A westward-flowing component of the Antarctic Slope Current (ASC) has also been identified in the eastern Ross Sea, which is a possible contributor to the external canyon levee's asymmetrical structure (Orsi and Wiederwohl, 2009; Miramontes et al., 2020).

2. Methods

2.1. Data collection and shipboard physical properties measurements

IODP Hole U1525A was cored to a depth of 208.28 m below seafloor (mbsf) through Plio-Pleistocene sediments. Here we focus on the interval between 0 and 121.05 mbsf, which was selected to provide a representative view of changing palaeoenvironmental conditions at Site U1525 across the Pleistocene. Coring primarily used the advanced piston corer and half-length advanced piston corer, although the extended core barrel was also used to drill through over-compacted sediments between 43 and 55.7 mbsf (McKay et al., 2019a). Cores were scanned on-board for magnetic susceptibility (pass-through and point-source),

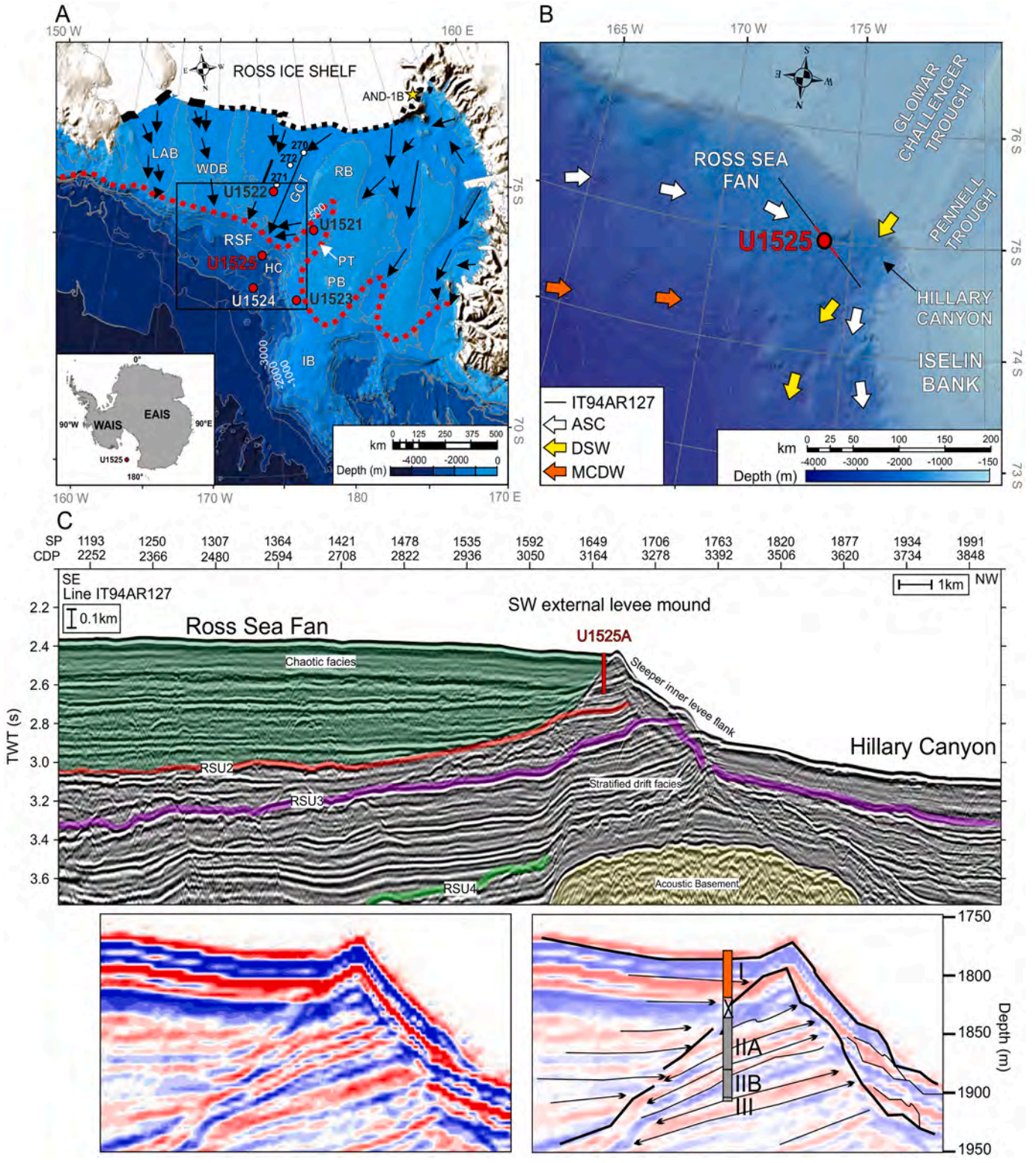

(caption on next page)

Fig. 1. Bathymetric maps of the Ross Sea, Antarctica. Map A shows the locations of Expedition 374 drill sites (red circles), current ice front location (black dashed line), palaeo-grounding line during the last glacial maximum (LGM; red dashed line) and palaeo-ice flow direction (black arrows) (adapted from Halberstadt et al., 2016 and Lee et al., 2017). GCT = Glomar Challenger Trough; HC = Hillary Canyon; IB = Iselin Bank; PB = Pennell Bank; PT = Pennell Trough; RB = Ross Bank; RSF = Ross Sea Fan. White circles 270–272 represent sediment cores DSDP-270-272 from Deep Sea Drilling Program Leg 28 (Hayes et al., 1973). Yellow star is Antarctic Drilling Project (ANDRILL) sediment core AND-1B (Naish et al., 2009). Inset map shows location of Site U1525 in relation to Antarctica: EAIS = East Antarctic Ice Sheet and WAIS = West Antarctic Ice Sheet. The location of Map B is shown in the black box. Map B shows a more detailed view of Site U1525 as outlined in the dashed box in Map A where ASC = Antarctic Slope Current; DSW = Dense Shelf Water and MCDW = Modified Circumpolar Deep Water (Budillon et al., 2011; Orsi and Wiederwohl, 2009). Bathymetric data is sourced from the International Bathymetric Chart of the Southern Ocean spaced at A) 500 m and B) 100 m intervals (IBCSO; Arndt et al., 2013). Multichannel seismic line IT94AR-127 is shown in C (Finetti et al., unpubl. Data; available from the Antarctic Seismic Data Library System). Collected using 2 × 20 air gun (71.96 L) and 1500 m streamer at a 50 m shot interval. Adapted from McKay et al., 2019b. Highlighted green unit shows TMF facies above RSU2. Yellow unit shows location of acoustic basement. SP = Shot Point; CDP = Common Depth Point; TWT = Two-way travel time. Box Ci shows a zoomed-in, depth converted profile of line IT94AR-127 from where Hole U1525A was extracted. Box Cii shows the same profile with black lines and arrows showing our interpretation. The location of Hole U1525A and its principal lithostratigraphic units are also shown. Unit I is highlighted in red to show the boundary between the Ross Sea Fan deposits and the external levee mound deposits below (Units II and III). The section filled with a cross below Unit I represents an interval of no core recovery. (For interpretation of the references to colour in this figure legend, the reader is referred to the web version of this article.)

gamma-ray attenuation (GRA) bulk density and natural gamma radiation (NGR). High-resolution core images were taken using a line-scan camera (20 pixels/mm). Discrete ~10cm^3 sediment samples were extracted at approximately 75 cm intervals for the purposes of calculating grain density and porosity. Unless otherwise specified, the core depth below sea floor method A(CSF-A) depth scale is reported here as mbsf. Detailed information on the methods used during Expedition 374 can be found in McKay et al. (2019a).

Table 1
Sedimentary facies observed in the top 121.05 m of Hole U1525A, based on grain size characteristics, visual core description and physical properties. Lithostratigraphic units used follow McKay et al., 2019b. For full lithological descriptions, see Supplementary Information.

Lithostratigraphic Unit (McKay et al., 2019b)	Facies Abbreviation	Facies Name	Lithological Description	Facies Interpretation
I	MDm	Massive muddy diamict	Grey, massive, diatom-bearing diamict with occasional large dropstones and some slight bioturbation in the uppermost 10 m. Matrix very poorly sorted fine sandy muds.	Debris flow deposition of subglacial or grounding-line proximal diamict from shelf. Deposited during margin-proximal glacials.
I	MDs	Stratified muddy diamict	Very stiff, dark brown to light yellowish brown, diatom-bearing, weakly-stratified diamict with very large cm-scale clasts and sharp upper (+lower?) contacts. Matrix very poorly sorted fine sandy muds.	Debris flow deposition of subglacial or grounding-line proximal diamict from shelf. Deposited during margin-proximal glacial. IRD influence?
IIA	Ms(A)	Mud with Type A silt laminae and dispersed clasts	Mode 1: Greenish-grey, strongly Type A-laminated diatom-bearing mud.	Frequent low-density turbidity current deposition. Deposited during margin-proximal glacials/deglaciations
			Mode 2: Greenish-grey, weak to rare Type A laminated mud with rare dispersed clasts and grey cm-scale muddy diamicts with sharp upper contacts. Fine to medium silt matrix interbedded on cm to dm-scale with intervals of coarser silt/very fine sandy mud. Rare bioturbation.	Infrequent low-density turbidity current deposition. Hemipelagic suspension settling: fine-grained material + IRD rainout. Deglacial/Interglacial.
IIA/IIB	Mm	Massive mud	Greenish-grey, massive fine to medium silty muds with rare dispersed mm-scale clasts and rare bioturbation.	Hemipelagic suspension settling: fine-grained material + occasional IRD rainout. Sea ice? Interglacial.
IIA	SDi	Interbedded diatom-bearing muddy diamict/sandy mud and foraminifera-bearing clast-rich sandy diamict	Light yellowish-brown foraminifera-rich muddy fine to medium sands to sandy mud with gradational contacts, interbedded on the dm-scale with faintly Type A laminated sandy-mud or muddy diamict.	Intense IRD + pelagic rainout of foraminifera (+bottom current winnowing of fine-grained material). Infrequent low-density turbidity current deposition. Interglacial (/full glacial collapse).
IIB	Ms(B)	Mud with Type B silt and gravel laminae and dispersed clasts	Mode 1: Greenish-grey, strongly Type B-laminated diatom-rich mud with dispersed clasts, and gravel layers. Infrequent slight to heavy bioturbation.	Bottom current winnowing Hemipelagic suspension settling: fine-grained material + IRD rainout Sea ice? Deglacial/Interglacial
			Mode 2: Greenish-grey, faintly/weakly Type B-laminated diatom-rich mud with dispersed clasts, gravel layers and cm-scale diamicts. Common slight to heavy bioturbation.	Weak bottom current winnowing Hemipelagic suspension settling: fine-grained material + Sea ice? IRD rainout Distal Glaciation/Deglacial
III	MDi	Interbedded mud and muddy diamict	Greenish-grey cm-scale, diatom-rich diamict interbedded on cm to dm-scale with faintly Type B-laminated diatom-rich mud. Heavily bioturbated in places, and contains dispersed clasts/gravel layers.	Hemipelagic suspension settling: fine-grained material + intense IRD rainout Weak bottom current winnowing Distal Glaciation/Deglacial

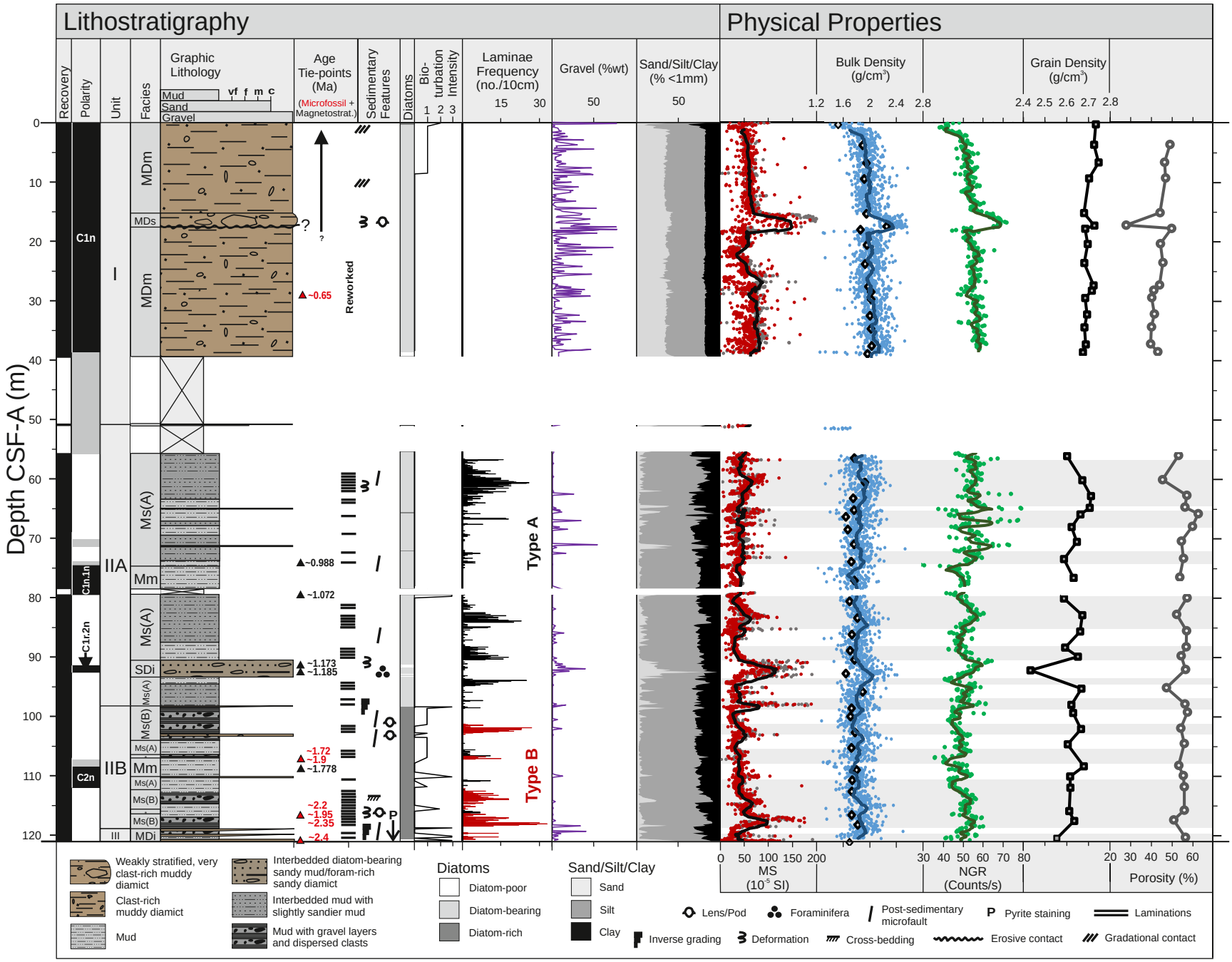
Lithostratigraphy
Physical Properties
Depth CSF-A (m)
Recovery
Polarity
Unit
Facies
Graphic Lithology
Mud
Sand
Gravel
vf f m c
Age Tie-points (Ma)
(Microfossil + Magnetostrat.)
Sedimentary Features
Diatoms
Bio-turbation Intensity
Laminae Frequency (no./10cm)
Gravel (%wt)
Sand/Silt/Clay (% <1mm)
Bulk Density (g/cm³)
Grain Density (g/cm³)
MDm
MDs
MDm
Ms(A)
Mm
Ms(A)
SDi
Ms(A)
Ms(B)
Ms(A)
Mm
Ms(A)
Ms(B)
Ms(B)
MDi
I
IIA
IIB
III
C1n
C1n.1n
C1r.2n
C2n
~0.65
~0.988
~1.072
~1.173
~1.185
~1.72
~1.9
~1.778
~2.2
~1.95
~2.35
~2.4
Reworked
Type A
Type B
P
MS (10⁻⁵ SI)
NGR (Counts/s)
Porosity (%)
Weakly stratified, very clast-rich muddy diamict
Clast-rich muddy diamict
Mud
Interbedded diatom-bearing sandy mud/foram-rich sandy diamict
Interbedded mud with slightly sandier mud
Mud with gravel layers and dispersed clasts
Diatoms
Diatom-poor
Diatom-bearing
Diatom-rich
Sand/Silt/Clay
Sand
Silt
Clay
Lens/Pod
Foraminifera
Post-sedimentary microfault
Pyrite staining
Laminations
Inverse grading
Deformation
Cross-bedding
Erosive contact
Gradational contact

Fig. 2. Detailed lithostratigraphic interpretation of Hole U1525A (0–121.05 mbsf CSF-A), modified from McKay et al., 2019b. Purple line is gravel wt% of whole sediment sample. Sand/silt/clay is %wt <1 mm fraction. Frequency of Type A and Type B laminae are shown in black and red respectively. Physical properties data includes: section half multi-sensor core logger (SHMSL; red circles) and whole round multi-sensor core logger (WRMSL) magnetic susceptibility (grey circles), black trend line = WRMSL 50-point running mean; GRA (light blue circles) and discrete wet bulk density (grey-filled diamonds), blue trend line = GRA 50-point running mean; green trend line = NGR 10-point running mean from McKay et al., 2019b. Core recovery, polarity, age tie-points, sedimentary features, diatom abundance and bioturbation intensity also from McKay et al., 2019b. See McKay et al., 2019b for full magnetostratigraphy. Light grey bars highlight intervals of lamination to aid comparison. (For interpretation of the references to colour in this figure legend, the reader is referred to the web version of this article.)

2.2. Grain size analysis

Grain size analyses for 0–121.05 mbsf were conducted using a Malvern Mastersizer 2000 laser particle size-analyser with an autosampler. Four subsamples of approximately $8mm^3$ (approx. 0.1 g) of sediment were dry sieved through a 1 mm mesh, treated with a 10% H_2O_2 solution to remove organic material and placed in a water bath at 60 °C overnight to assist the reaction process. A 10% solution of sodium hexametaphosphate was added to the Mastersizer wet sample dispersion unit and 40 s of ultrasound was applied to disperse material before measurement. Samples were analysed using an absorption coefficient of 0.005 and refractive index of 1.53. Coarse material was then manually dry-sieved in a nested stack at half-phi intervals (between 1.4 and 63 mm). Ice-rafted debris (IRD) was characterised as material larger than 1 mm in diameter, unless the unit was subsequently identified as a mass flow. The grain size boundaries used for clay, silt and sand in the laser particle size analysis are <4 μm (clay), 63 μm (silt) and 63-1000 μm (very fine-coarse sand), respectively. The classification scheme used for sediment nomenclature and colour can be found in McKay et al. (2019a). The term 'mud' is used as a descriptor for sediments with a mixture of silt and clay where neither size class dominates (i.e. <80% silt, or < 80% clay) as per the sediment nomenclature scheme.

2.3. Laminae analysis

Laminae were classified into two categories on the basis of visual observations (e.g. thickness, colour and boundary characteristics), which are referred to as 'Type A' and 'Type B' (see Table 1 and Sections 3.4 and 3.5 for descriptions of laminae types). Grain size was not used as an identification factor as analyses showed both types of laminae are predominantly coarse silts. Measurements were taken from the core midpoint at the base of the lamina to the nearest millimetre. Type B laminae 'packages' were counted as single laminae due to the fine-scale nature and discontinuity of laminae enclosed within (Sections 3.4 and 3.5).

2.4. Age model

We use the shipboard age model for Site U1525 that uses magnetic reversal stratigraphy, supported by biostratigraphic datums from published Southern Ocean zonations (Fig. 2) (McKay et al., 2019a). These utilised the first appearance and last appearance datum of marine diatom and radiolarian species. Palaeomagnetic reversals were correlated to the Gradstein et al. (2012) geomagnetic polarity timescale, which are calibrated using marine magnetic anomaly profiles (Hilgen et al., 2012; Lourens et al., 2004). The interval of Unit III discussed in this paper (118.58–121.05 mbsf; ~2.4 Ma) and Subunits IIA/B are early-mid Pleistocene (~2.4 Ma to ~0.8 Ma). Unit I is of mid-Late Pleistocene age (<~0.8 Ma). The shipboard age model includes two interpreted unconformities. Unconformity 1 (U1) is present within the interval of no recovery between 38.83 and 55.7 mbsf. Drilling parameters were used to determine when the bit penetrated the base of the over-compacted sediments and suggest that the unconformity is likely present near the base of this interval (McKay et al., 2019b). Unconformity 2 (U2) is present near the base of the studied interval at ~112 mbsf. The thickness of Unit I is fully constrained, however the base of the unit was not piston-cored due to the presence of consolidated or coarse material in the sequence. Drilling parameters (e.g. rate of penetration, weight on bit) infer that Unit I exists down to ~55.7 mbsf, as piston coring was able to resume only after these parameters indicate sediments were soft enough to penetrate with a piston core. This is unlike U2, which is not well constrained in the depth domain but is thought to cover a longer time interval than U1 (~1.95–2.4 Ma; McKay et al., 2019b).

3. Results

3.1. Core overview

We refine the preliminary lithofacies classification scheme from McKay et al., 2019b into seven lithofacies, which are summarised in Table 1 and Figs. 2–3, and described in more detail in the Supplementary Information. We describe these seven lithofacies in the context of the three primary lithostratigraphic units that were identified during initial shipboard core analysis (McKay et al., 2019b). Unit I (0–51.11 mbsf), Unit II (51.11–118.58 mbsf), which is further divided into Subunits IIA and IIB, and Unit III (118.58–208.27 mbsf/base of hole). The boundary between Subunit IIA and IIB is located at 98.2 mbsf (Figs. 2, 3). The principal lithologies identified in this core are diamict and mud.

3.2. Unit I facies

Unit I contains muddy diamict and is mostly grey, diatom-bearing, unconsolidated and massive, here referred to as facies MDm, with a ~ 2 m-thick interval of stiff and weakly stratified muddy diamict, facies MDs, between 15.28-17.64 mbsf (Fig. 2, Table 1). Grain size analyses of the two facies in Unit I reveal similar matrix particle size distributions, both of which are also distinctly richer in gravel and sand than the underlying units (Figs. 4, 5a/b/c). Both facies in Unit I show percentages of average mud (silt and clay; 55wt%) sand (32wt%) and gravel (13wt%) content comparable to diamicts recovered from other Antarctic TMFs, such as on the Belgica and Weddell Sea slopes (Melles, 1991; Hillenbrand et al., 2009a; Gales et al., 2018). The percentage of clay is mostly uniform in Unit I (average 18% of <1 mm fraction), as most of the variation in grain size is seen in the percentage of silt and sand (Fig. 2). Facies MDs is very stiff and is similar to stratified diamicts recovered from the Prydz Bay TMF (Passchier et al., 2003). The matrix is also slightly sandier than in facies MDm, and it also contains a number of larger sub-angular to sub-rounded clasts (Figs. 2, 4, 5c).

3.3. Unit II facies

Unit II is located below U1 and contains a strikingly different lithology to Unit I. Sediments are composed of mostly greenish-grey, massive to laminated diatom-bearing/rich muds. Unit II also contains a higher and more variable amount of clay (average 25% of <1 mm fraction) than Unit I, and is rich in post-depositional soft sediment deformation features such as cm-scale micro-faulting, as well as cm-scale diamicts and matrix-supported gravel layers (Table 1; Figs. 6, 7, 8). Magnetic susceptibility, bulk density and NGR show lower average values than in Unit I (Fig. 2). Five facies in Unit II have been identified in this study: mud with 'Type A' silt laminae and dispersed clasts, Ms(A) (Figs. 6a/b, 7b, 8); massive mud, Mm (Figs. 6c, 7a); interbedded diatom-bearing muddy diamict/sandy mud and foraminifera-bearing clast-rich sandy diamict, SDi (Fig. 6d); and mud with 'Type B' silt laminae, gravel layers and dispersed clasts, Ms(B) (Figs. 7c/d, 8). Gravel in these layers is mostly angular to sub-rounded and between 1 mm - 4 mm in diameter, with occasional larger clasts up to 11 mm in size.

3.4. 'Type A' lamina in facies Ms(A)

Type A laminae are planar, normally graded and have sharp lower contacts that show truncation of underlying sediments (Fig. 9). In facies Ms(A), there are two main modes of Type A lamination: a) Mode 1: strongly interlaminated mud with silt laminae, and b) Mode 2: faintly-laminated mud interbedded with cm-scale sandy muds or muddy diamicts (Table 1; Figs. 6a/b, 7b, 8). Laminae in interlaminated intervals are rarely thicker than 1–2 mm, evenly spaced (1–5 mm) and usually decrease in frequency towards the upper and lower limits of the interlaminated intervals. The majority of sampled Type A laminae are coarse silts, but are occasionally very fine-grained sand in the rarer, thicker lamina (>1 cm; Figs. 4, 8). Clasts are rarely found within strongly laminated intervals (Mode 1) but are more common in the muddier sections of Mode 2.

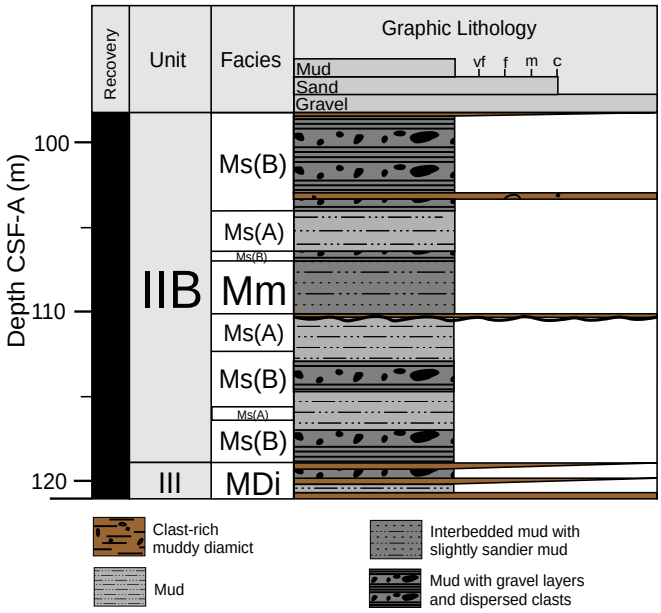

Fig. 3. Expanded view of facies in Subunit IIB/ Unit III.

3.5. 'Type B' laminae in facies Ms(B)

Silty Type B laminae in this interval are characteristically distinct from those in facies Ms(A) and exhibit sharp upper and lower contacts with no grading (Fig. 9). Furthermore, gravel layers and dispersed clasts are common between instances of Type B laminae. Many laminae are exceptionally thin (1–2 mm), although very fine, stacked, mm-scale discontinuous laminae form packages up to 1 cm thick (Fig. 8). Similarly to facies Ms(A), facies Ms(B) is composed of a) Mode 1: more strongly-laminated intervals and b) Mode 2: areas of less frequent lamination that commonly shows slight to heavy bioturbation (Table 1, Fig. 2). Matrix-supported, gravel-rich layers are common in both modes of this facies, ranging in thicknesses from 1 mm-1 cm and with mostly gradational, occasionally sharp lower contacts.

3.6. Unit III facies

The 2.47 m of Unit III between 118.58 and 121.05 mbsf included in this study is assigned to facies MDi, which is diatom-rich, cm- to dm-scale diamict interbedded with muds containing dispersed clasts and silt/gravel laminae (Figs. 10a/b, 11). It contains average clay values (23% of <1 mm fraction) similar to Unit II (Fig. 2). The boundary between Unit II and III does not appear to be accompanied by a stratigraphic unconformity, with U2 occurring slightly above this lithostratigraphic boundary at ~112 mbsf (McKay et al., 2019b). Gravel in layers is mostly angular to sub-rounded and between 1 mm - 4 mm in diameter, with occasional larger clasts up to 11 mm in size.

3.7. Frequency analysis

Three main diamict units are observed in Unit I, corresponding to changes in physical properties and visual characteristics, which are illustrated in Fig. 12 along with the frequency occurrence of Type A and B laminations. These diamicts are variable in thickness and in clast content. The thickest deposit, interval D1, is homogenous and displays little evidence of containing separate deposits. Interval D2 corresponds to the stiff diamict facies MDs, and interval D3 sits directly above U1.

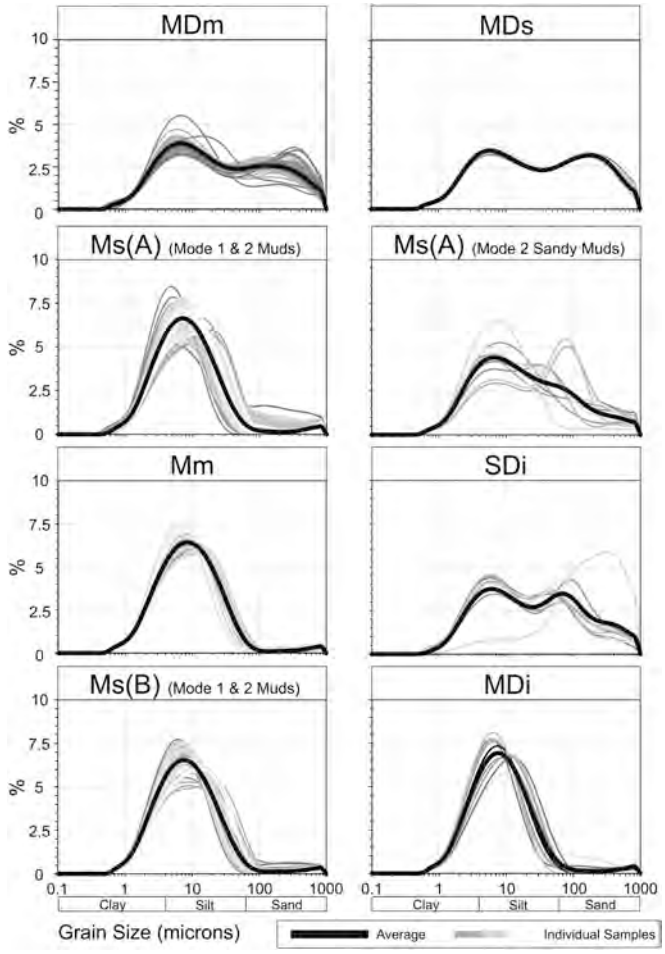

Fig. 4. Matrix grain size distributions for facies identified in U1525A: Massive Muddy Diamict, MDm; Stratified Muddy Diamict, MDs; Mud with Type A Silt Laminae and Dispersed Clasts, Ms(A); Massive Mud, Mm; Interbedded Diatom-bearing Muddy Diamict/Sandy Mud and Foraminifera-bearing, Clast-rich Sandy Diamict, SDi; Mud with Type B Silt and Gravel Laminae and Dispersed Clasts, Ms(B); and Interbedded Mud and Muddy Diamict, MDi. Distributions for laminated facies Ms(A) and Ms(B) do not include samples taken from laminae, only the matrix distribution. See supplementary information for more description on Modes 1&2 for facies Ms(A) and Ms(B).

Diamicts in Unit II and III are thinner and separated from one another by several metres of other sediment types. The most distinct Unit II diamict is interval D6 (facies SDi), interbedded between muddy diatom-bearing diamict/sandy muds and foraminifer-bearing sandy diamicts. Most diamicts in units II and III are found in the diatom-rich Subunits IIB and Unit III (intervals D8–12), whereas the two main deposits in Subunit IIA (intervals D4–5) directly succeed thin, diatom-rich mud intervals (Figs. 2, 12).

Laminated sediments show distinct, high-frequency intervals of both Type A and Type B laminae occurring in a waxing-waning pattern (Fig. 12). Type A laminae (normally-graded silt or very fine sand laminae with erosive bases) are present throughout all of Unit II, whereas Type B (silt laminae with sharp upper and lower contacts, no grading) are found in Subunit IIB and III. Type A laminae are found primarily in Subunit IIA but are also weakly present in Subunit IIB after intervals of Type B lamination (Figs. 2, 12). Type B laminae are concentrated within five main intervals and display some of the highest frequencies of laminae in the core (33 laminae/10 cm). Some higher frequency intervals appear to succeed thin diamict intervals D8–10. Type B high frequency intervals between ~105–118 mbsf are also followed by short, low frequency intervals of Type A laminae.

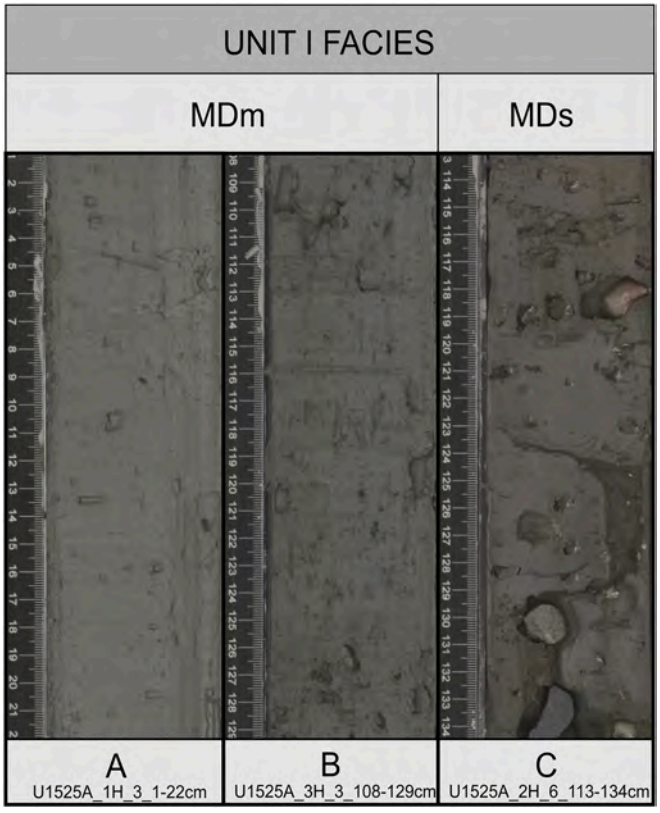

Fig. 5. Core images displaying facies in Unit I from: A) 3.01–3.22 mbsf; B) 22.19–22.4 mbsf and; C) 17.26–17.47 mbsf. Massive Muddy Diamict, MDm (A, B), displays varying amounts of clast content as demonstrated in A and B. C displays facies MDs.

Type A laminae are concentrated into 4 main intervals above ~95 mbsf, and mostly show greater spacing between high-frequency intervals than peaks in Type B laminae frequency. Type A interlaminated intervals are therefore thicker than interlaminated intervals of Type B. The thickest interlaminated interval in U1525A is found between ~57–64 mbsf, which lies between interval D4 and U1.

4. Facies Interpretation

4.1. Facies MDm

Facies MDm (D1, D3) are interpreted here as glacigenic debris flows due to their size, lithological structure, high clast content and matrix grain size distribution. The occurrence of these deposits in Hole U1525A are indicative of upper slope failure driven by ice grounded at the continental shelf break as inferred for other high-latitude margins (e.g. Laberg and Vorren, 1996; Vorren and Laberg, 1997; Tripsanas and Piper, 2008). Periods of intense ice-rafting and the subsequent rainout of entrained IRD may also deposit diamict on polar continental slopes; however, these deposits are often thin, stratified, texturally heterogeneous, and possess gradational contacts (Kurtz and Anderson, 1979). Furthermore, the lack of microfossils in MDm could suggest that source sediments were likely deposited close to or further inland of the grounding line, away from open marine conditions favourable to biological activity (Anderson et al., 1984; Licht et al., 1999; Prothro et al., 2018). This would discount ice-rafting as the sole process responsible for coarse material in Unit I. Facies MDm displays characteristics (soft, massive, muddy diamict) similar to glacigenic debris flow deposits identified on other Antarctic continental margins, such as in the Bellingshausen and Weddell Seas (Kurtz and Anderson, 1979; King et al., 1998; Passchier et al., 2003; Hillenbrand et al., 2009a; Gales et al.,

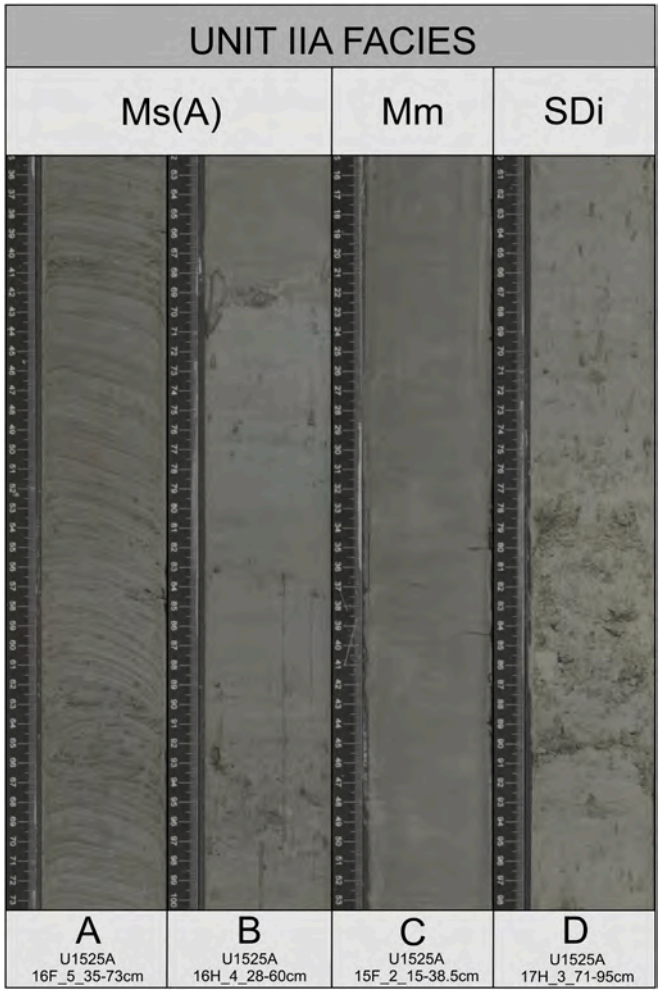

Fig. 6. Core images displaying facies in Subunit IIA from: A) 83.81–84.19 mbsf; B) 85.5–85.88 mbsf; C) 76.11–76.49 mbsf; D) 92.12–92.5 mbsf. Mode 1 and 2 of facies Ms(A) are shown in A) strongly Type A-interlaminated mud with silt laminae, and B) weakly Type A-laminated mud interbedded with cm-scale sandy muds or diamicts (see Table 1 for in-depth facies description). Images C and D show facies Mm and SDi, respectively.

2018). Soft diamicts may develop primarily on the outer shelf in a number of depositional settings, such as deformed subglacial diamicts, grounding line-proximal diamicts, and iceberg-turbated diamicts (Domack, 1990; Licht et al., 1999). Sediment cores from Deep Sea Drilling Project (DSDP) Sites 270, 271 and 272 extracted from the Glomar Challenger Trough reveal a ~ 19 m-long microfossil-barren Pleistocene sub-unit of 'sand-silt-clay with pebbles', Unit 1B, which includes a significant fraction (<20wt%) of sand (Fig.1; Barrett, 1975). The textural characteristics of DSDP-270-272 Unit IB are reflected in the bimodal muddy-sand matrix of diamicts in Hole U1525A Unit I, indicating that facies MDm sediments likely originated on the shelf and were reworked through mass-wasting downslope (Fig.4).

4.2. Facies MDs

Similarly to MDm, facies MDs (D2) is interpreted to be the result of a debris flow event following the delivery of large volumes of sediment to the continental shelf edge. However, the unique characteristics of facies MDs (extremely stiff, low porosity, browner colour, slightly sandier matrix, increased clast size range and content) indicate that the associated mass flow possessed different rheological properties to those in facies MDm, and/or was subject to transformative processes after

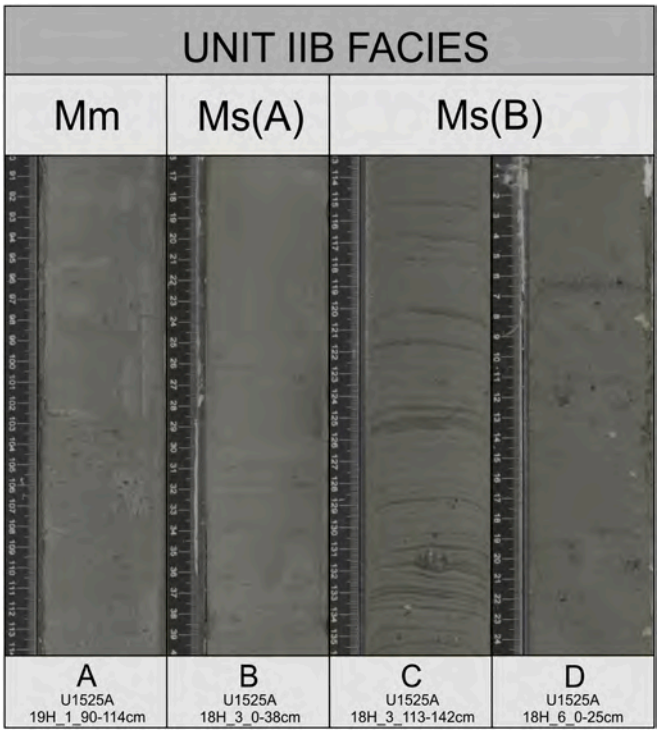

Fig. 7. Core images displaying facies in Subunit IIB from: A) 108.6–108.84 mbsf; B) 105.4–105.64 mbsf; C) 102.32–102.55 mbsf; and D) 101.19–101.44 mbsf. Images A and B show facies Mm and Ms(A), respectively. Mode 1 and 2 of facies Ms(B) are shown in C) strongly Type B-interlaminated mud with silt laminae, and D) weakly Type B-laminated diatom-rich mud with dispersed clasts, gravel layers and cm-scale diamicts (see Table 1 for in-depth facies description).

deposition on the slope. The browner colour of facies MDs could indicate a change in clay mineralogy or iron oxide minerals (e.g. hematite) as it does not coincide with changes in biogenic content, has a high magnetic susceptibility and higher values of NGR (Wei et al., 2014). Clay minerals possess diverse properties affecting sediment dilatancy, cohesion, compaction and sediment yield stress, which is the minimum shear stress required to initiate flow (Hampton, 1975; Mulder et al., 1997; Yu et al., 2013). This change in sediment colour may be an indicator of variable sediment source input (Andrews and Jennings, 1987). Sediment entrainment within the basal shear zone may be the cause of reduced clast size and content towards the lowermost ~15 cm of the facies (Lowe, 1982; Laberg and Vorren, 2000). Thus, weak stratification probably occurred during the debris flow event as a result of surface substrate deformation and not from depositional and/or erosional processes on the continental shelf.

4.3. Facies Ms(A)

We interpret Type A laminae in facies Ms(A) as low-density turbidity current deposits mobilised on the upper slope of the Hillary Canyon, following facies models of fine-grained turbidites (Lowe, 1982; Stow and Piper, 1984; Shanmugam, 1997). Turbidites with similar characteristics (barren, IRD-sparse, interlaminated mud containing normally-graded silt or very fine sand laminae with erosive bases; Fig. 9) have been documented at several locations around the Antarctic continental margin, indicating rapid deposition of sediments under energetic seabed conditions (Pudsey, 2000, 2002; Lucchi et al., 2002; Lucchi and Rebesco, 2007; Cowan et al., 2008; Caburlotto et al., 2010). Grain size spectra of Type A laminae (Fig. 8) show low concentrations of sand and characteristic modes in the medium-coarse silt fraction that are similar to deposits created by overbank spilling of turbidity currents identified

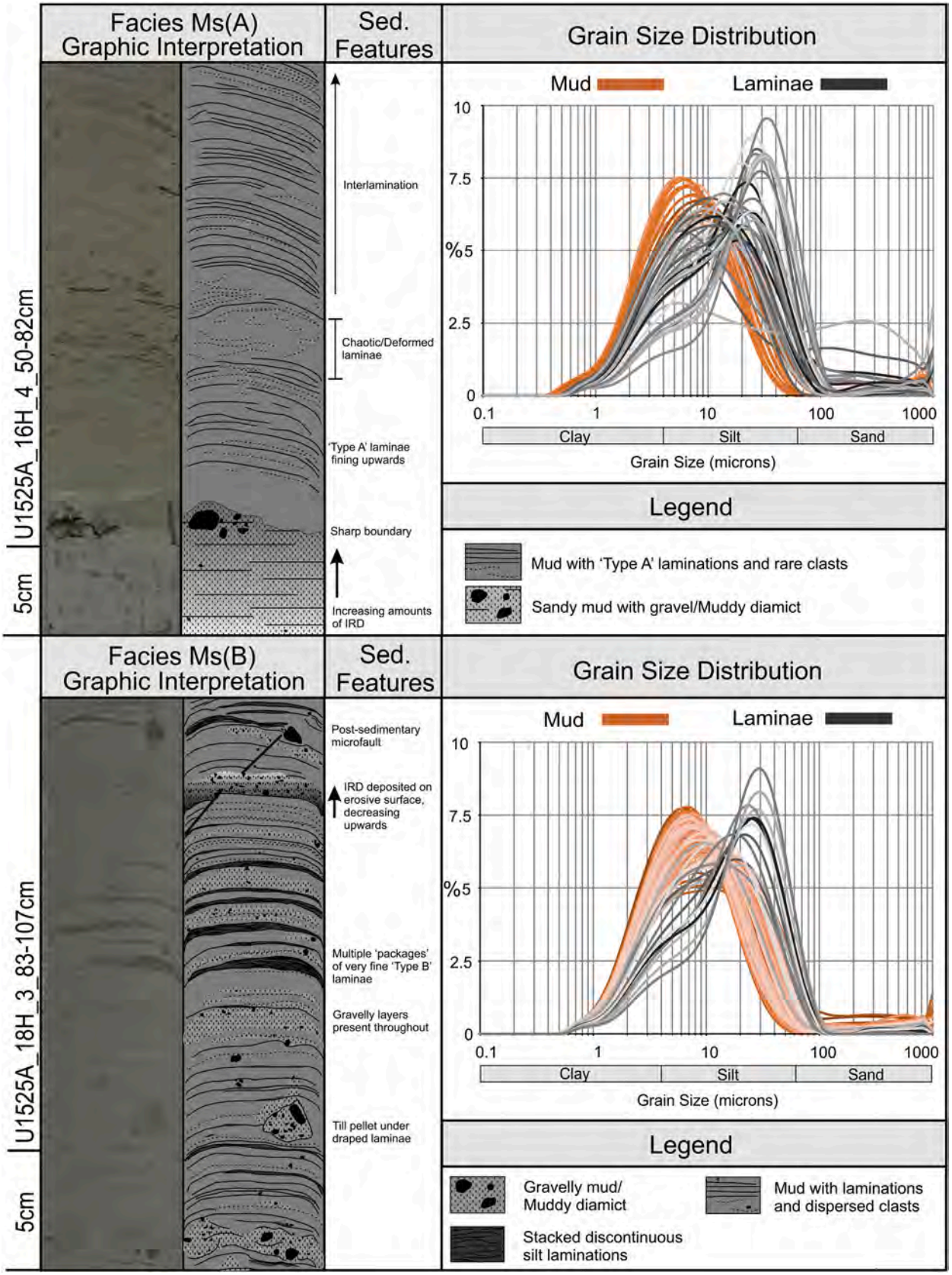

Fig. 8. Characteristics of laminated intervals in Unit II including interpreted illustration of sedimentary features and texture from Mud with Type A Silt Laminae and Dispersed Clasts facies, Ms(A) (83.96–84.29 mbsf) and Laminated Mud with Type B Silt Laminae and Gravel Layers facies, Ms(B) (102.02 m-102.26 mbsf). Grain size spectra for laminae (grey) and mud (orange) include all samples taken from facies Ms(A) and facies Ms(B).

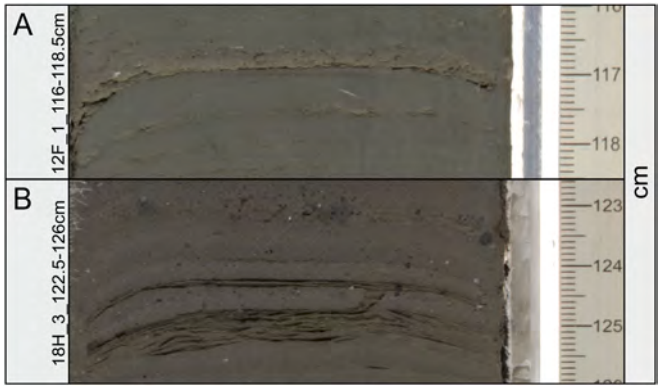

Fig. 9. Closeup images of the two styles of lamination found in U1525A where A = 'Type A' laminations (61.56–61.585 mbsf) and B = 'Type B' laminations (102.415–102.45 mbsf).

Fig. 10. Core images displaying facies MDi in Unit III from A) 118.54–118.64 mbsf and B) 119.96–120.28 mbsf.

on the Labrador Sea slope (Chough and Hesse, 1980; Wang and Hesse, 1996) and the Pacific margin of the Antarctic Peninsula (Lucchi et al., 2002). High frequency intervals of Type A laminae may therefore represent overbank deposits from turbidity currents that have spilt over the crest of the external Hillary Canyon levee during glacial periods (Fig. 13). Overbanking is a process that is likely restricted to the inner flank and crest of the external levee (Piper and Normark, 1983; Peakall et al., 2000). Therefore, given Site U1525's location on the outer flank of the external canyon levee, Type A laminae may be the settled remains of fine-grained sediment that have been flow-stripped from turbidity currents mobilised on the inner levee flank (Peakall et al., 2000; Sinclair and Tomasso, 2002).

Low-density turbidity currents may have deposited sediment rapidly enough to account for the lack of distinct IRD packages and bioturbation in Type A interlaminated intervals (Wang and Hesse, 1996; Lucchi et al., 2002; Lucchi et al., 2013). This could explain why gravel in Mode 1 of facies Ms(A) is rare and dispersed (Table 1). Furthermore, grounded ice terminating at the shelf break, as well as other small fringing ice shelves, are likely to have released comparatively 'cleaner' icebergs containing less entrained debris in comparison with inland outlet glaciers only exposed to ocean calving during interglacial periods (Smith et al., 2019). The four main episodes of high turbidity current activity recorded in Subunit IIA may therefore reflect the incidence of subglacial sediment release at the shelf break in this section of the eastern Ross Sea. Peaks in turbidite (Type A) frequency found prior to ~1.1 Ma are closer together and shorter in sequence, whereas the large peak after ~1.1 Ma suggests a much more prolonged period of turbidity current deposition (Figs. 2, 12).

In facies Ms(A) Mode 2, the grey muddy diamicts (intervals D4–5, 9)/sandy muds with sharp upper contacts were likely deposited as glacimarine diamict resulting from increased glacial calving and retreat and subjected to winnowing. This is in line with interpretations of IRD-rich hemipelagic sediments from other Antarctic continental margins (Pudsey, 2000, 2002; Passchier et al., 2003; Lucchi and Rebesco, 2007; Caburlotto et al., 2010; Patterson et al., 2014).

4.4. Facies Mm

Facies Mm is interpreted as interglacial sediment deposited through hemipelagic processes, including rainout of fine-grained terrigenous material suspended in the water column. The characteristics of facies Mm (greenish grey, lacking bioturbation and rare IRD) are not typical of interglacial sediments, which are usually identified as bioturbated, sandy muds that are browner in colour and contain IRD (Wang and Hesse, 1996; Pudsey, 2002; Hillenbrand et al., 2009b; Passchier et al., 2011; Patterson et al., 2014). Evidence of warmer oceanographic conditions or increased productivity in these interglacial sediments is not clearly reflected in microfossil content (i.e., no obvious change in % diatoms, foraminifera or calcareous nannofossils; Fig. 2). This suggests that, during interglacial periods, biological material was not preserved in the fossil record due to their composition; for example, algae such as *Phaeocystis* do not produce fossil remains (Goffart et al., 2000), or it was removed prior to or following deposition through physical and/or chemical processes, e.g. test dissolution due to a shallow carbonate compensation depth (Fillon, 1975). Plumite mud beds with characteristics similar to facies Mm (structureless or some faint colour contrasts with no textural variation, sparse IRD and lacking bioturbation) are observed on the eastern Prydz Bay margin, East Antarctica, and the Antarctic Peninsula (Pudsey and Camerlenghi, 1998; Passchier et al., 2003; Lucchi and Rebesco, 2007). However, pure plumite facies may have a seaward limit of no more than tens of kilometres from the ice margin on the shelf and are attributed to meltwater plume release from glacial advance or retreat (Hesse et al., 1997; Lucchi et al., 2002).

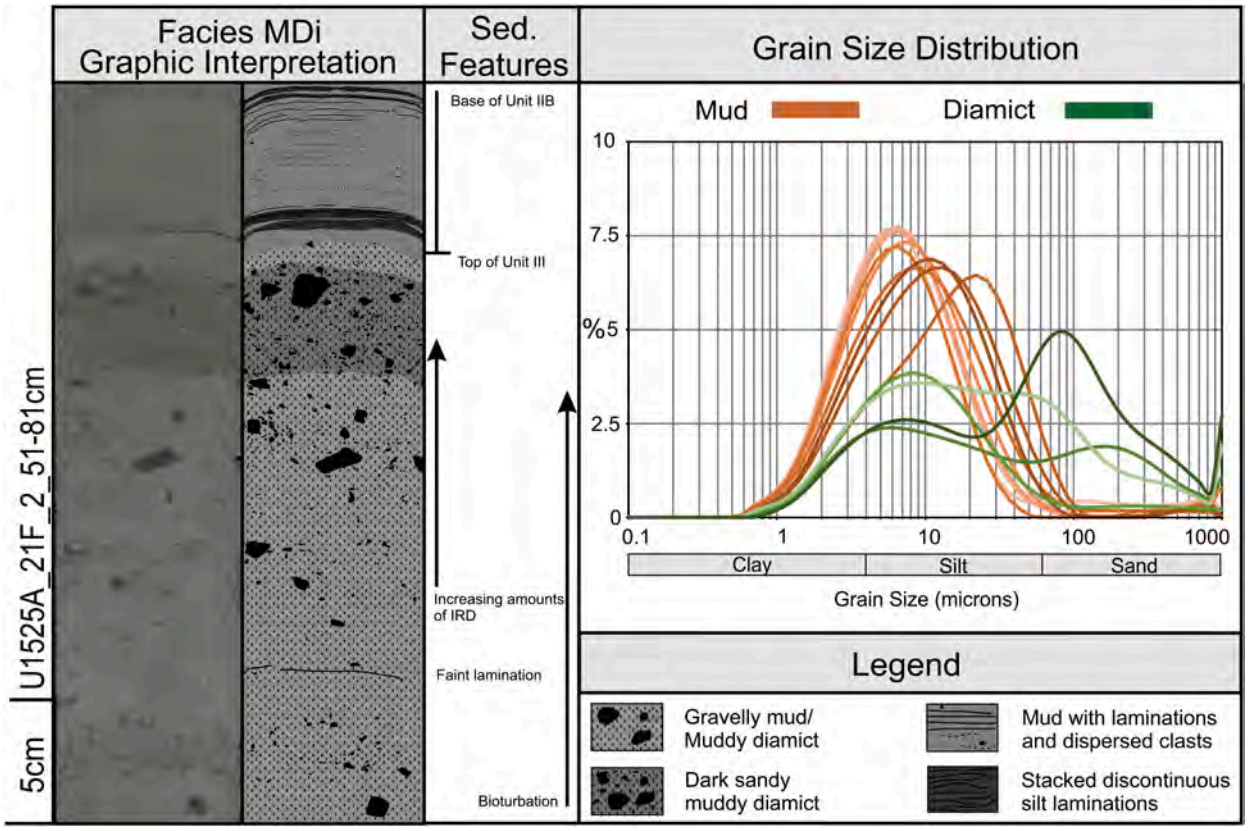

Fig. 11. Characteristics of sediments in Unit III including interpreted illustration of sedimentary features and texture from Interbedded Mud and Muddy Diamict, facies MDi (118.51–118.80 mbsf) and grain size distribution spectra for diamicts (green) and mud (orange) from all samples in facies MDi. (For interpretation of the references to colour in this figure legend, the reader is referred to the web version of this article.)

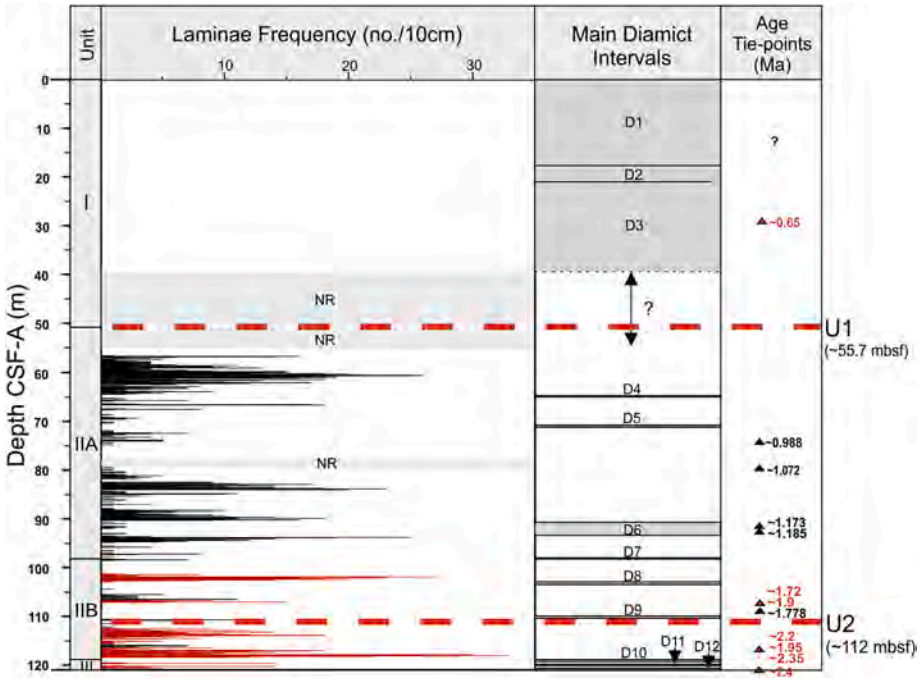

Fig. 12. Graph showing expanded view of laminae frequency against occurrence of diamict intervals in Hole U1525A (D1–12). Type A laminae are represented by black bars. Type B laminae are red. NR = intervals of missing sediment recovery. Thin black dashed line in main diamict interval column reflects uncertainty over size of diamict interval due to non-recovery of sediment. Red dashed lines show locations of chronostratigraphic unconformities interpreted in McKay et al., 2019b (U1 and U2). Age tie-points as in Fig. 2. (For interpretation of the references to colour in this figure legend, the reader is referred to the web version of this article.)

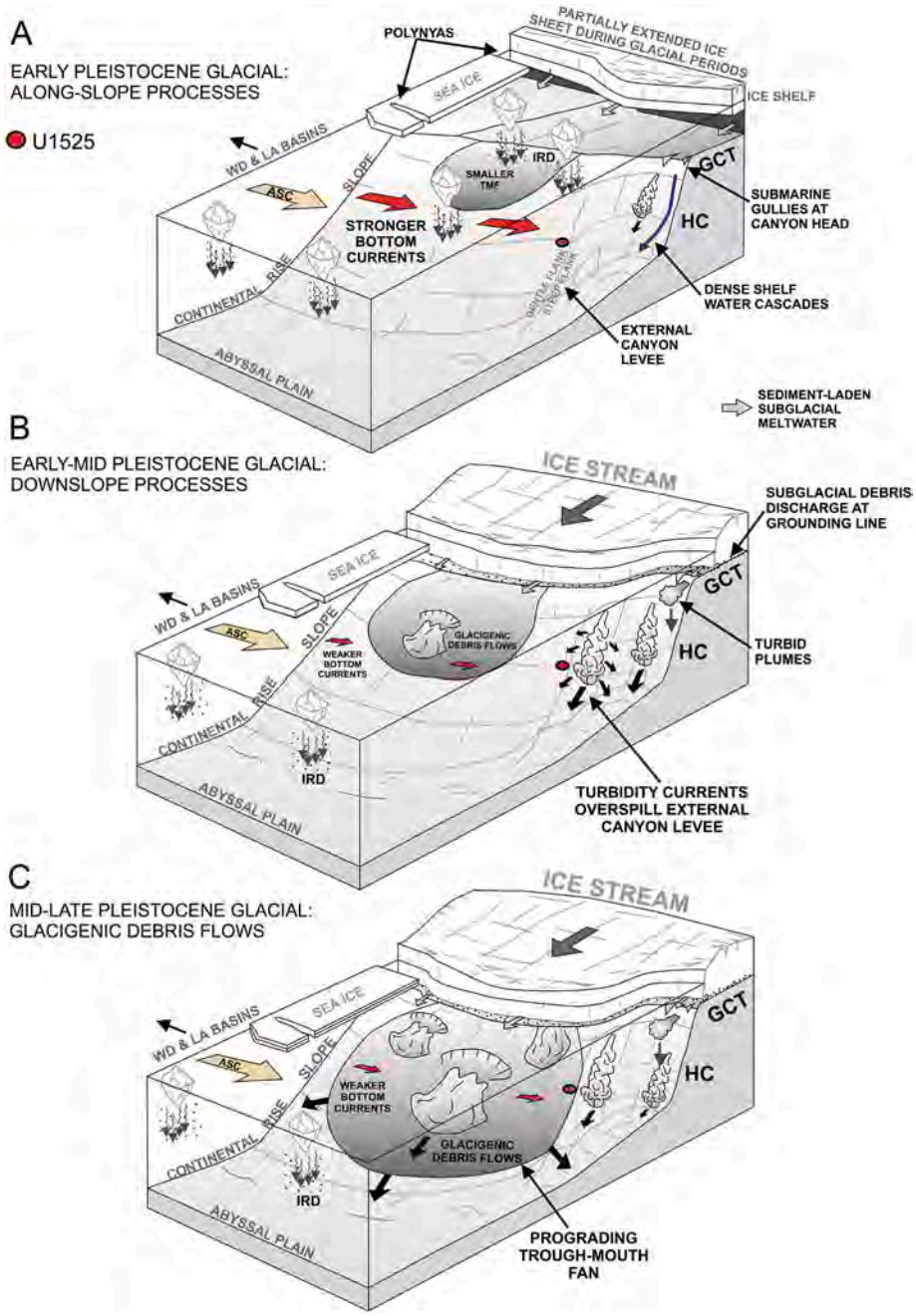

Fig. 13. Conceptual diagrams showing differences between glacial period scenarios for: A) early Pleistocene; B) early-mid Pleistocene; and C) mid-late Pleistocene. Red circle represents IODP Site U1525. Red arrows show relative strength of bottom currents. Light blue arrows show release of sediment-laden subglacial meltwater. ASC = Antarctic Slope Current; GCT = Glomar Challenger Trough; HC = Hillary Canyon; TMF = Trough-mouth Fan; WD & LA = Whales Deep and Little America Basins. (For interpretation of the references to colour in this figure legend, the reader is referred to the web version of this article.)

4.5. Facies SDi

Facies SDi (interval D6; Fig. 12) is unique in Hole U1525A and is here interpreted as possible evidence of glacial collapse, based on the presence of planktonic foraminifera and high amounts of sand and gravel (Figs. 2, 4). A diverse benthic assemblage was also found in this facies (McKay et al., 2019b). Foraminifera in Ross Sea sedimentary sequences are usually indicative of sea-ice free, open marine interglacial conditions, as planktonic species are relatively sparse in the continental shelf waters and increase in abundance seawards on the slope and rise (Majewski et al., 2018). The coarse grain size of facies SDi may be a joint result of rapid emplacement of IRD and increased bottom current velocity. Strongly interlaminated turbidite intervals (Mode 1 of Facies Ms (A), described in Section 3.4) are also missing in facies SDi, providing further evidence of the absence of proximal grounded ice (Fig. 2). The diatom-bearing muddy diamict/sandy mud intervals interbedded between each foraminifera-bearing sandy deposit could suggest that glacial collapse occurred in a series of large-scale calving events that were punctuated by brief periods of glacial re-advance.

4.6. Facies Ms(B)

Silty Type B laminae found in Unit III and Subunit IIB are interpreted as deposits influenced by geostrophic current activity. The characteristics of Type B laminae (<2 mm thickness, sharp upper and lower contacts, no grading; Fig. 9), along with the presence of dispersed clasts and gravelly IRD layers in the diatom-rich facies Ms(B), reflect previous descriptions of muddy glacial contourites (Piper and Brisco, 1975; Pudsey, 2000; Lucchi and Rebesco, 2007; Passchier et al., 2011). Grain size distributions for muds in facies Ms(B) display a dominant mode at ~7.8 μm (Figs. 4, 8), whereas Type B laminae are slightly coarser at ~10–11 μm. Together with the laminae characteristics (horizontal,

wispy and fine-grained) and other sedimentary structures (i.e. thicker laminae 'packages'), these lithological features suggest an alternating but relatively low to moderate current strength where deposition dominates over winnowing (Pudsey, 2000; Rebesco et al., 2014). Evidence of deposition under a lower-energy environment in facies Ms(B) is further supported by the presence of laminae draping over clasts and minor bioturbation (Fig. 8; Sup. Info), although sediments mostly lack bioturbation. Minimal bioturbation may explain why Type B laminated intervals in facies Ms(B) Mode 1 are relatively well-preserved, particularly in laminae 'packages'. This is in agreement with laminated contourites found in sediment drifts off the Pacific margin of the Antarctic Peninsula, where Lucchi and Rebesco (2007) suggested that climatically influenced reductions in deep water oxygenation, and a longer seasonal duration of sea-ice cover into the summer months acted to suppress primary productivity, explaining the lack of bioturbation. Type B laminations in Subunit IIB show larger peaks in frequency towards the base of the unit, reflecting a more prolonged period of bottom current activity before ~1.7 Ma (Fig. 12). The on/off style of Type B lamination frequency potentially relates to changing bottom current intensity over time, with peaks in frequency representing periods of time where current speed increased (Stow et al., 2002; Lucchi and Rebesco, 2007). Gravel/IRD layers show an episodic input of IRD in Subunit IIB, suggesting pulse-like delivery of IRD to the site (Fig. 8). Bioturbated diamicts in Ms(B) Mode 2 (D7–8) are also consistent with IRD-rainout and resemble intervals D4–5 (Sections 3.4 and 3.7). As the large quantity of IRD layers deviate from the 'end-member' description of glacial contourites, facies Ms(B) is probably a hybrid deposit resulting from sustained bottom current activity coupled with hemipelagic settlement of IRD and fine-grained sediments suspended in the water column.

4.7. Facies MDi

Coarse sand and gravel in facies MDi are interpreted as IRD deposited by a mixture of slow, sustained rainout from calved icebergs (sparse IRD) and large pulses of IRD delivery (IRD-rich layers) from increased melting and grounded ice retreat. This interpretation is in alignment with IRD deposits identified from Scoresby Sund, East Greenland, and the Antarctic Peninsula (Dowdeswell et al., 1994; Lucchi et al., 2002). Muddy intervals and weak laminae are also present in this facies, although in much thinner stratigraphic intervals, suggesting that similar along-slope processes responsible for facies Ms(B) also operated to deposit facies MDi. Bioturbated, inversely-graded diamicts interbedded with weakly-laminated mud in this facies (D10–12) suggests deposition in a hemipelagic environment with strong influence from IRD rainout. D10-D12 are therefore interpreted as possible gravel-lag deposits winnowed by periodic strengthening of bottom currents as described in Stow et al. (2002) and Rebesco et al. (2014).

5. Discussion

5.1. Along-slope influenced processes (Units II and III)

Regional interpretations of seismic and seabed bathymetry data have shown large sediment drifts building on the Hillary Canyon external levees (Fig. 1c), with seabed morphology indicating that strong northwest-flowing bottom currents exist (De Santis et al., 1999; De Santis et al., 2015; Kim et al., 2018; McKay et al., 2019b; Conte et al., 2021). The presence of contourites is supported by modern in-situ oceanographic observations from the western flank of the Hillary Canyon that shows down- and along-slope bottom currents with velocities of up to 15 cms^{-1} (Jacobs et al., 1970; Bergamasco et al., 2002; Orsi and Wiederwohl, 2009; Budillon et al., 2011). Given that bottom current-influenced facies Ms(B) was likely deposited under low current speeds, Site U1525 may have been exposed to weak along-slope bottom current flow during the early Pleistocene, rather than to higher current velocities. This is consistent with modern oceanographic measurements suggesting that the greatest current velocities in the Hillary Canyon are currently focussed higher on the upper slope (Budillon et al., 2011). Variations in the along-slope current speed that are potentially responsible for the on/off style of Type B lamination could relate to changes in the strength and/or location of the along-slope current core (Rebesco et al., 2014), which is supported by evidence of variable along-slope current speeds and contourite deposition on the Iselin Bank since the late Miocene (Conte et al., 2021). Instability of along-slope currents likely resulted from movement of the ice front through glacial-interglacial cycles and/or shifting patterns of Westerly winds. Within muddy intervals such as facies Mm (Subunit IIA/B), which can extend up to 3.0 m thick in sequence, the absence of strong interlamination could imply prolonged periods of reduced geostrophic and gravity-driven bottom current activity during interglacial periods.

At Site U1525, benthic activity may have been inhibited due to reduced ventilation of shelf waters, as sea ice reduced vertical mixing of deep ocean water masses such as Circumpolar Deep Water (CDW) (Patterson et al., 2014; Stein et al., 2020). Low concentrations of benthic foraminifera and other microfossils associated with strengthened ventilation and upwelling, or open-marine conditions, in facies Mm and Ms(B) supports this; however, it should be noted that the modern calcite compensation depth in the Ross Sea is shallow (≤430 m), which inhibits the preservation of calcareous foraminifera (Kennett, 1968). The presence of microfossil-barren glacial contourite facies Ms(B) therefore may imply the influence of longer duration seasonal sea-ice into the summer months, and subsequent restricted ventilation of shelf water masses that feed oxygenated bottom water to Site U1525.

Suspended fine-grained material originating from other canyon systems to the southeast (e.g. Whales Deep & Little America Basins, Fig. 1a–b) may have been laterally advected to the site via weak along-slope currents and Coriolis forcing, potentially delivering sediment from several sources on the shelf. For example, meltwater plumes entrained in currents may travel up to ~130 km away from their source (Hesse et al., 1997). Furthermore, nepheloid layers are common on the Ross Sea margin and have been observed at water depths exceeding 1500 m below sea level around the Hillary Canyon (Jacobs et al., 1970; Budillon et al., 2006; Capello et al., 2009). Settlement from re-suspended fine-grained glacimarine sediment discharge at the grounding line therefore likely supplied much of the fine-grained sediment at Site U1525 in Units II-III. These processes may have also remained relevant into the late Pleistocene, however sediments in Unit I are anticipated to have undergone significant reworking. The early Pleistocene (~2.4 Ma to ~1.4 Ma; Subunit IIB/ Unit III) depositional environment at Site U1525 is therefore envisaged to be a greater function of reworking by the along-slope bottom current component, rather than gravity-driven bottom currents or mass wasting. However, the original sediment supply to these water depths prior to bottom current reworking may have been driven by downslope processes.

5.2. Down-slope influenced processes (Unit II)

Turbidity currents deposits found in Mode 1 of facies Ms(A) were probably initiated by sediment loading on the upper slope from the release of subglacial debris, as well as sediment-laden subglacial meltwater, from the base of margin-proximal and retreating grounded ice on the shelf (e.g. Ó Cofaigh et al., 2003; Noormets et al., 2009). Evidence for extensive turbidity current activity exists in deeply-incised gully systems along the shelf edge at the Hillary Canyon head, which were likely formed over multiple glacial cycles by erosive turbidity currents (Gales et al., 2021). Considering the location of Site U1525 on the canyon flank (Fig. 1), the absence of high-energy sedimentary features e.g. cross-stratification or rip-up clasts in facies Ms(A), could suggest that the main body of turbidity currents were centred in the Hillary Canyon. This hypothesis is supported by seismic interpretations of contourite drifts from the western flank of the Hillary Canyon suggesting that the formation of the canyon levees occurred prior to the Pleistocene (McKay

et al., 2019b; Conte et al., 2021).

After ~1.4 Ma (Subunit IIA and above) where facies Ms(A) is most common, the preservation of turbidites suggest that bottom current reworking ceased or significantly decreased. Flow-stripping could also explain why Type A laminae are less abundant in Subunit IIB, as fine-grained sediment suspended via flow-stripping could have been winnowed away from the site as a combined result of stronger geostrophic current activity enhanced by Coriolis forcing (Wang and Hesse, 1996). This may exclude a secondary hypothesis for Type B interlamination as a product of gravity-driven and along-slope processes acting contemporaneously, as is observed on many polar continental margins (Kuvaas and Leitchenkov, 1992; Michels et al., 2001; Rebesco et al., 2007; Mulder et al., 2008). The waxing-waning style of Type B laminae peaks are similar to Type A, which could suggest they are the remains of turbidity currents winnowed by stronger along-slope bottom currents (Andersen et al., 1996; Escutia et al., 2000, 2003). Whilst we anticipate that a complex interplay of processes contributed towards sedimentation in most, if not all facies in Hole U1525A, our interpretation of Type A laminae as deposits from turbidity currents initiated when ice was more proximal to the shelf break contradicts this hypothesis.

Turbidity currents initiated as a result of margin-proximal ice depositing sediment at the shelf break do not explain the presence of weak, less frequent (<10 laminae/10 cm) and discontinuous Type A laminae in the 2.4 to 1.4 Ma (Subunit IIB) interval of Hole U1525A, which occur after peaks in Type B laminations (Fig. 12). Site U1525 was likely located north of the Ross Sea TMF during the early Pleistocene, until the TMF prograded over the core site (see Section 5.4). Hence, some turbidites may also represent the distal portion of debris flows operating on the TMF as flow transformation occurs via the progressive entrainment of water into the debris flow body over distance (Fisher, 1983; Stow, 1985; Stow and Smillie, 2020). The lack of turbidite interlamination (facies Ms(A) Mode 1; Table 1), and lack of debris flow deposits in Subunit IIB suggest that episodes of grounded ice advance to the shelf break, if they occurred, were either significantly reduced in a) frequency and/or b) duration of fully-extended conditions (Fig. 12). Periodic WAIS advances are documented in AND-1B across all of the Plio-Pleistocene (Naish et al., 2009), although these data from Hole U1525A suggest that very few of these advances likely reached the shelf break. When the WAIS was not under full glacial conditions, turbidity currents may also have been triggered by other mechanisms, such as cascading dense shelf water or slope failure relating to isostatic rebound processes; however, the relationship between sediment gravity flows and cascades is not well defined (Figs. 2, 11) (Bart et al., 1999; Canals et al., 2006). Gravity-driven overflows of dense shelf water cascade over the shelf break in highly localised regions such as the Hillary Canyon, as well as passively in smaller submarine canyons along the eastern Ross Sea margin (Amblas and Dowdeswell, 2018; Bergamasco et al., 2002; Jacobs, 1991; Jacobs and Haines, 1982). High amounts of cascading dense shelf water, turbidity currents, and hyperpycnal flows at the mouths of other canyon systems along the margin (including the Hillary Canyon) could contribute towards the resuspension of fine sediments and maintenance of a nepheloid layer (Escutia et al., 2000, 2005; De Santis et al., 2003; Donda et al., 2003). Persistent, intense periods of dense shelf water cascading could mobilise low-density sediment gravity flows on the Hillary Canyon slope, if sediment were able to accumulate on the slope over extended periods of time (Gales et al., 2021). However, the modern oceanographic setting shows that the Coriolis force drives dense shelf water to cascade further towards the western area of the Hillary Canyon (Budillon et al., 2011; Morrison et al., 2020; Gales et al., 2021). Assuming this was also the case during the early-mid Pleistocene, and that slope/shelf break palaeobathymetry did not impede along-slope current activity in the Hillary Canyon, turbidity currents resulting from cascading may therefore not have occurred close enough to the core site to influence sedimentation to a significant degree at Site U1525. Consequently, a sedimentary sequence covering the same time interval drilled on the opposite canyon flank is anticipated to differ from the sequence recorded at Site U1525, possibly to a great extent.

The increased frequency of Type A interlamination after ~1 Ma is likely due to a prolonged grounded ice presence at the margin during the Mid-Pleistocene Transition (MPT; ~1 Ma), interpreted as a time when most ice sheets, including the WAIS, increased in size, covering longer, asymmetrical 100 kyr glacial/interglacial cycles rather than the obliquity-forced, symmetrical 41 kyr cycles seen previously (Tziperman and Gildor, 2003; Lisiecki and Raymo, 2005; Naish et al., 2009; Pollard and DeConto, 2009).

5.3. Ice rafted debris (Units II and III)

Icebergs calving into the eastern Ross Sea are typically deflected westwards with wind and surface water current direction (Keys and Fowler, 1989), supplying IRD from multiple locations along the ice front in the Ross Sea and also potentially from further to the east. The gravel-rich intervals D4–12 found in Mode 2 of facies Ms(A)/Ms(B) and facies MDi that are interpreted as periods of sustained IRD deposition during deglacial periods therefore likely contain IRD from several bedrock source regions. IRD-sparse interglacial facies Mm may highlight changing iceberg pathways, possibly relating to reduced transport from further east by the ASC or polynyas near the shelf break acting to divert icebergs away from the core site during interglacials. However, current and iceberg drift patterns would mostly be regulated by palaeobathymetry and the ASC. Alternatively, it could indicate relative stability of the ice sheet margin during these periods if the transference of heat and fresh water through water mass exchange across the shelf break was also stable (Lucchi et al., 2002; Budillon et al., 2011).

5.4. Glacially-induced debris flows (Unit I)

The three main diamict intervals identified in Unit I (D1–3; facies MDm and MDs) may reflect the frequency occurrence of debris flows at the site, however more work is needed to constrain this further (Fig. 12). Due to the location of Site U1525 on the upper slope, debris flows of sufficient size and erosional capacity likely entrained the uppermost layer of sediment, bypassing and redistributing deglacial and interglacial sediments towards the outer margins of the fan and the continental rise (Laberg and Vorren, 2000). This accounts for the lack of contouritic deposits, turbidites, or hemipelagic deposits usually associated with sedimentation on TMFs between full glacial periods (Vorren and Laberg, 1997). The shift to glacigenic debris flow-dominated sedimentation is a probable result of continued TMF progradation across the gently-sloping flank of the Hillary Canyon external levee, in response to the increased delivery of subglacial material to the shelf break and aided by gravitational settling from subglacial meltwater plumes (Fig. 13). Delivery and melt-out of subglacial debris by ice sheet advance to the shelf edge, alongside sediment-laden subglacial meltwater release likely contributed towards the continued progradation of the TMF (Tripsanas and Piper, 2008; Lucchi et al., 2013).

Diamicts across the Ross Sea continental shelf show consistency in matrix grain size despite variable bedrock sources (Perotti et al., 2017; Halberstadt et al., 2018), therefore increased influence of ice-rafting could explain why more sand is present in the sediment matrix of facies MDs without an associated reduction in clay. Before remobilisation, diamict temporarily stored on the upper slope as a glacial wedge by grounded ice at the margin may have had a longer residence time prior to slope failure (Laberg and Vorren, 1995), and was subsequently subjected to a greater influence of glacimarine or ice-rafted deposition. It is therefore also conceivable that facies MDs is the result of changing grounded ice-stream dynamics delivering sediments from differing upstream bedrock sources. Ice flow switching occurred in the Ross Sea in response to variations in East and West Antarctic Ice Sheet dynamics, and drainage changes on other WAIS-controlled continental shelves have occurred during the late Quaternary (Mosola and Anderson, 2006; Hillenbrand et al., 2009b; Greenwood et al., 2012). Terminal moraines

on the eastern Ross Sea shelf have also shown a pre-LGM grounding event that displays a major shift in WAIS ice stream direction from west to north (Bart, 2004; Böhm et al., 2009). Further investigation of clast and clay mineral provenance could provide useful insight into the origin of facies MDs.

5.5. Further considerations: results from other Antarctic marine drill cores

5.5.1. Early Pleistocene (Marine Isotope Stage 31, ~1.1 Ma)

The variety of species within the benthic assemblage in facies SDi points towards changing bottom water conditions, with winnowing of smaller planktonic tests (<250 μm) implying strengthened bottom current speeds possibly related to intensified wind-driven along-slope flow of the ASC (McKay et al., 2019b). This enhanced ASC flow may have allowed more intrusions of relatively warm, nutrient-rich CDW further onto the Ross Sea continental shelf through Ekman pumping, reducing sea ice production due to heat supply, enhancing basal melt in the ice shelf cavity and providing more favourable biological conditions (Anderson et al., 1984; Morrison et al., 2020). Diatomite in AND-1B and a carbonate-rich unit from Cape Roberts Project drill core CRP-1, both dated to Marine Isotope Stage 31 (MIS 31) age (1.1 Ma), reflect warmer-than present, sea-ice free oceanographic conditions and increased carbonate preservation in the western Ross Sea (Scherer et al., 2008; Naish et al., 2009; McKay et al., 2012; Villa et al., 2012; Teitler et al., 2015). Similar carbonate-rich beds have been identified at IODP Sites U1359 and U1361 from the Wilkes Land margin (Escutia et al., 2011; McKay et al., 2011; Beltran et al., 2020), and from ODP Sites 1165–1167 in Prydz Bay (Villa et al., 2008). This suggests that the drivers for the depositional anomaly of facies SDi in Hole U1525A occur in adjacent sectors of the Antarctic margin and are not a result of a localised process. Modelling studies informed by Ross Sea shelf drill core interpretations have shown an almost complete collapse of the WAIS occurred during MIS 31 and earlier Pleistocene interglacials, which would have translated into high calving rates and the subsequent release of large amounts of IRD into the Ross Sea (DeConto et al., 2012).

5.5.2. The Mid-Pleistocene transition and the following period (<1 Ma)

Our interpretation of increased turbidity current deposition at Site U1525 relating to enhanced ice cover on the continental shelf after ~1 Ma is supported by AND-1B facies that suggest MIS 31 was the last clear evidence of WAIS retreat and open water conditions at AND-1B. After ~1 Ma, the AND-1B core is dominated by subglacial diamictites during glacial maxima, and thin mudstone units during interglacials (McKay et al., 2009, 2012). This was interpreted as a baseline shift in climate state across the MPT whereby ocean temperatures cooled enough to allow large ice shelves to persist through interglacial periods (McKay et al., 2012), which in turn promoted ice sheet stability through the buttressing effect provided by ice shelves (Weertman, 1974). Subglacial deformation features in the diamictites from AND-1B indicate grounded ice sheets expanded into the Ross Sea during the glacial maxima of the past 0.8 Ma. It should also be noted that no turbidite beds are found in the C1n.1n subchron (Jaramillo) in Hole U1525A (Fig. 2), which coincides with the last well-constrained evidence of WAIS collapse at AND-1B (Naish et al., 2009).

6. Conclusions

We identified seven facies using grain size and facies analysis of sediment cores collected from Hole U1525A in the eastern Ross Sea. These facies correspond to differing depositional mechanisms affected by oceanographic conditions and grounded WAIS dynamics on the continental shelf (Table 1) (McKay et al., 2019b). They also provide insight into the relative contributions of processes occurring in the Hillary Canyon and the Ross Sea TMF to the depositional environment on this sector of the slope. The Pleistocene (<~2.4 Ma) sedimentary sequence at Site U1525 can therefore be divided into three key intervals:

- Early Pleistocene (~2.4 Ma to ~1.4 Ma) Units III and Subunit IIB: IRD-and diatom-rich, slightly bioturbated facies with fine-scale 'Type B' interlamination, which are interpreted as contourites formed by along-slope bottom current winnowing, suggesting a higher influence of bottom currents at Site U1525 during the early Pleistocene relative to later time intervals. Lateral advection of fine-grained sediments by along-slope bottom currents and Coriolis forcing likely delivered sediments from other canyon systems further to the East of the site. Interglacial sediments are characteristically lacking in bioturbation and microfossils.
- Early-mid Pleistocene (~1.4 Ma to ~0.8 Ma) Subunit IIA: 'Type A' laminations are interpreted as flow-stripped turbidity current deposits focussed in the Hillary Canyon. Strongly interlaminated turbidite intervals are suggested to form as high amounts of subglacial debris and sediment-laden subglacial meltwater released from a proximal grounding line are deposited and contribute towards slope instability. Other processes, such as cascading dense shelf water or isostatic rebound, may have initiated turbidity currents outside of glacial periods. A distinct sandy interval containing large amounts of ice-rafted material and foraminifera-bearing layers indicates open marine conditions around ~1.18 Ma, a depositional anomaly that is also noted in mid-Pleistocene interglacials of Wilkes Land and Prydz Bay regions (Villa et al., 2008; Escutia et al., 2011; Beltran et al., 2020). This could reflect a period of enhanced ASC flow towards the continental shelf, which led to strengthened inflow of CDW and periodic glacial collapse during the mid-Pleistocene (1.18–1.0 Ma). The largest interval of turbidite lamination occurs after ~1 Ma, consistent with more prolonged/frequent grounded ice presence at the shelf break leading into the MPT.
- Mid-late Pleistocene (<0.8 Ma) Unit I: Onset of glacigenic debris flow sedimentation on this sector of the upper slope, developing from large volumes of subglacial diamict and IRD delivered to the margin. A slightly sandier and more clast-rich stiff diamict facies potentially reflects variable clay mineralogy and a longer residence time on the upper slope before remobilisation. Debris flows possessed sufficient erosional capacity to remove the previous interglacial sequence. Colder conditions and frequent fully-extended glacial conditions allowed the continued progradation of the TMF across the core site.

Our conceptual model derived from a semi-continuous continental slope record in the eastern Ross Sea identifies increasing frequency of glacial advances to the shelf edge as a result of increased Antarctic cooling over the Pleistocene, particularly after the MPT. We also identify that during periods of reduced ice sheet extent of the early- to mid-Pleistocene, the depositional setting is characterised by contouritic currents that we hypothesise represent a stronger ASC and enhanced upwelling of warm sub-surface CDW onto the continental shelf. This led to increased frequency and extent of ice sheet retreat at that time. The results presented here form a strong basis for future work, where testing of these hypotheses based on the physical properties of the sediment can be conducted by geochemical and palaeontological proxies at Site U1525 and other IODP Expedition 374 sites (U1523 and U1524). Such an approach will allow us to identify how shifts in current speed and sediment delivery to the continental shelf break more directly relates to shifting surface and deep water mass properties through the Plio-Pleistocene. These data will help provide fundamental new insights into how oceanic processes near Antarctica's continental shelf edge have contributed to the triggering of past marine-based ice sheet retreat. This work also provides valuable context for regional seismic interpretations and in-depth studies of the Ross Sea TMF formation.

Declaration of Competing Interest

None.

Acknowledgements

This research used samples and data provided by the International Ocean Discovery Program (IODP). We thank the members of IODP Expedition 374 Science Party and the captain and crew of the *JOIDES Resolution*. JSL acknowledges the support from European Consortium for Ocean Research Drilling and the Research Council of Norway allowing for his participation on Expedition 374 and the post-cruise work. RMM was funded by the Royal Society of New Zealand (New Zealand) Te Apārangi Marsden Fund (grant 18-VUW-089) and the MBIE (New Zealand) funded Antarctic Science Platform (ANTA1801). JG was funded by the Natural Environment Research Council (United Kingdom) (grant NE/R018189/1). LD was funded by the Italian Antarctic Research Program (Italy) PNRA16_00016 project. DKK was funded by US National Science Foundation (United States) (grants OCE-1326927 and OPP-2000995). All Expedition 374 shipboard datasets are publicly available via the following link: https://web.iodp.tamu.edu/OVERVIEW/. The multichannel seismic profile reprocessed by Riccardo Geletti (OGS) for the IODP Exp. 374 and used in this work is available at the Antarctic Seismic Data Library System (https://sdls.ogs.trieste.it) under the auspices of the Scientific Committee on Antarctic Research (SCAR) policy.

References

Alonso, B.A., J., B., Díaz, J.I., Bartek, l.r., 1992. Pliocene-Pleistocene seismic stratigraphy of the Ross Sea: evidence for multiple ice sheet grounding episodes. In: Elliot, D.H. (Ed.), Contributions to Antarctic Research III, 57, pp. 93–103.

Alonso, B., Ercilla, G., Casas, D., Stow, D.A.V., Rodríguez-Tovar, F.J., Dorador, J., Hernández-Molina, F.-J., 2016. Contourite vs gravity-flow deposits of the Pleistocene Faro Drift (Gulf of Cadiz): sedimentological and mineralogical approaches. Mar. Geol. 377, 77–94. https://doi.org/10.1016/j.margeo.2015.12.016.

Amblas, D., Dowdeswell, J.A., 2018. Physiographic influences on dense shelf-water cascading down the Antarctic continental slope. Earth Sci. Rev. 185, 887–900. https://doi.org/10.1016/j.earscirev.2018.07.014.

Andersen, E.S., Dokken, T.M., Elverhøi, A., Solheim, A., Fossen, I., 1996. Late quaternary sedimentation and glacial history of the western Svalbard continental margin. Mar. Geol. 133 (3), 123–156. https://doi.org/10.1016/0025-3227(96)00022-9.

Anderson, J.B., Brake, C.F., Myers, N.C., 1984. Sedimentation on the Ross Sea Continental Shelf, Antarctica. Mar. Geol. 57, 295–333. https://doi.org/10.1016/0025-3227(84)90203-2.

Andrews, J.T., Jennings, A.E., 1987. Influence of sediment source and type on the magnetic susceptibility of fiord and shelf deposits, Baffin Island and Baffin Bay, NWT. Can. J. Earth Sci. 24 (7), 1386–1401. https://doi.org/10.1139/e87-131.

ANTOSTRAT, 1995. Seismic stratigraphic atlas of the Ross Sea. In: Geology and Seismic Stratigraphy of the Antarctic Margin, 68.

Arndt, J.E., Schenke, H.W., Jakobsson, M., Nitsche, F.-O., Buys, G., Goleby, B., Rebesco, M., Bohoyo, F., Hong, J.K., Black, J., Greku, R.K., Udintsev, G.B., Barrios, F., Reynoso-Peralta, W., Taisei, M., Wigley, R., 2013. The International Bathymetric Chart of the Southern Ocean (IBCSO) - Digital Bathymetric Model. https://doi.org/10.1594/PANGAEA.805734.

Barker, P.F., Camerlenghi, A., 2002. Glacial history of the Antarctic Peninsula from Pacific margin sediments. In: Proc. ODP, Sci. Results, 178, pp. 1–40. https://doi.org/10.2973/odp.proc.sr.178.238.2002.

Barker, P.F., Barrett, P.J., Cooper, A.K., Huybrechts, P., 1999. Antarctic glacial history from numerical models and continental margin sediments. Palaeogeogr. Palaeoclimatol. Palaeoecol. 150 (3), 247–267. https://doi.org/10.1016/S0031-0182(98)00224-7.

Barrett, P.J., 1975. Textural characteristics of Cenozoic preglacial and glacial sediments at Site 270, Ross Sea, Antarctica. Initial Rep. Deep Sea Drill. Proj. 28, 757–767. https://doi.org/10.2973/dsdp.proc.28.1975.

Bart, P.J., 2004. West-directed flow of the West Antarctic Ice Sheet across Eastern Basin, Ross Sea during the Quaternary. Earth Planet. Sci. Lett. 228 (3–4), 425–438. https://doi.org/10.1016/j.epsl.2004.10.014.

Bart, P.J., Owolana, B., 2012. On the duration of West Antarctic Ice Sheet grounding events in Ross Sea during the Quaternary. Quat. Sci. Rev. 47, 101–115. https://doi.org/10.1016/j.quascirev.2012.04.023.

Bart, P.J., De Batist, M., Jokat, W., 1999. Interglacial collapse of Crary Trough-mouth fan, Weddell Sea, Antarctica; implications for Antarctic glacial history. J. Sediment. Res. 69 (6), 1276–1289. https://doi.org/10.2110/jsr.69.1276.

Beltran, C., Golledge, N.R., Ohneiser, C., Kowalewski, D.E., Sicre, M.-A., Hageman, K.J., Smith, R., Wilson, G.S., Mainié, F., 2020. Southern Ocean temperature records and ice-sheet models demonstrate rapid Antarctic ice sheet retreat under low atmospheric CO2 during Marine Isotope Stage 31. Quat. Sci. Rev. 228, 106069. https://doi.org/10.1016/j.quascirev.2019.106069.

Bergamasco, A., Defendi, V., Zambianchi, E., Spezie, G., 2002. Evidence of dense water overflow on the Ross Sea shelf-break. Antarct. Sci. 14 (3), 271–277. https://doi.org/10.1017/S0954102002000068.

Böhm, G., Ocakoğlu, N., Picotti, S., De Santis, L., 2009. West Antarctic Ice Sheet evolution: new insights from a seismic tomographic 3D depth model in the Eastern Ross Sea (Antarctica). Mar. Geol. 266 (1), 109–128. https://doi.org/10.1016/j.margeo.2009.07.016.

Brancolini, G., Busetti, M., Marchetti, A., Santis, L., Zanolla, C., Cooper, A., Cochrane, G., Zayatz, I., Belyaev, V., Knyazev, M., Vinnikovskaya, O., Hinz, F., 1995. Descriptive Text for the Seismic Stratigraphic Atlas of the Ross Sea, Antarctica, pp. 271–286.

Budillon, G., Gremes-Cordero, S., Salusti, E., 2002. On the dense water spreading off the Ross Sea shelf (Southern Ocean). J. Mar. Syst. 35 (3–4), 207–227. https://doi.org/10.1016/s0924-7963(02)00082-9.

Budillon, G., Salusti, E., Tucci, S., 2006. The evolution of density currents and nepheloid bottom layers in the Ross Sea (Antarctica). J. Mar. Res. 64 (4), 517–540. https://doi.org/10.1357/002224006778715739.

Budillon, G., Castagno, P., Aliani, S., Spezie, G., Padman, L., 2011. Thermohaline variability and Antarctic bottom water formation at the Ross Sea shelf break. Deep-Sea Research Part I-Oceanographic Research Papers 58 (10), 1002–1018. https://doi.org/10.1016/j.dsr.2011.07.002.

Caburlotto, A., Lucchi, R.G., De Santis, L., Macrì, P., Tolotti, R., 2010. Sedimentary processes on the Wilkes Land continental rise reflect changes in glacial dynamic and bottom water flow. Int. J. Earth Sci. 99 (4), 909–926. https://doi.org/10.1007/s00531-009-0422-8.

Canals, M., Puig, P., de Madron, X.D., Heussner, S., Palanques, A., Fabres, J., 2006. Flushing submarine canyons. Nature 444 (7117), 354–357. https://doi.org/10.1038/nature05271.

Capello, M., Budillon, G., Cutroneo, L., Tucci, S., 2009. The nepheloid bottom layer and water masses at the shelf break of the western Ross Sea. Deep-Sea Res. II Top. Stud. Oceanogr. 56 (13–14), 843–858. https://doi.org/10.1016/j.dsr2.2008.10.032.

Chough, S., Hesse, R., 1980. The Northwest Atlantic Mid-Ocean Channel of the Labrador Sea; III, Head spill vs. body spill deposits from turbidity currents on natural levees. Journal of Sedimentary Research 50 (1), 227–234. https://doi.org/10.1306/212F79B4-2B24-11D7-8648000102C1865D.

Conte, R., Rebesco, M., De Santis, L., Colleoni, F., Bensi, M., Bergamasco, A., Kovacevic, V., Gales, J., Zgur, F., Accettella, D., De Steur, L., Ursella, L., McKay, R., Kim, S., Lucchi, R.G., 2021. Bottom current control on sediment deposition between the Iselin bank and the Hillary canyon (Antarctica) since the late Miocene: An integrated seismic- oceanographic approach. Deep Sea Research Part I: Oceanographic Research Papers 103606. https://doi.org/10.1016/j.dsr.2021.103606.

Cooper, A.K., Barrett, P.J., Hinz, K., Traube, V., Letichenkov, G., Stagg, H.M.J., 1991. Cenozoic prograding sequences of the Antarctic continental margin: a record of glacio-eustatic and tectonic events. Mar. Geol. 102 (1), 175–213. https://doi.org/10.1016/0025-3227(91)90008-R.

Cowan, E.A., Hillenbrand, C.D., Hassler, L.E., Ake, M.T., 2008. Coarse-grained terrigenous sediment deposition on continental rise drifts: a record of Plio-Pleistocene glaciation on the Antarctic Peninsula. Palaeogeogr. Palaeoclimatol. Palaeoecol. 265 (3), 275–291. https://doi.org/10.1016/j.palaeo.2008.03.010.

Dangendorf, S., Hay, C., Calafat, F.M., Marcos, M., Piecuch, C.G., Berk, K., Jensen, J., 2019. Persistent acceleration in global sea-level rise since the 1960s. Nat. Clim. Chang. 9 (9), 705–710. https://doi.org/10.1038/s41558-019-0531-8.

De Santis, L., Anderson, J.B., Brancolini, G., Zayatz, I., 1995. Seismic record of late Oligocene through Miocene glaciation on the central and eastern continental shelf of the Ross Sea. In: Geology and Seismic Stratigraphy of the Antarctic Margin, 68, pp. 235–260. https://doi.org/10.1029/AR068p0235.

De Santis, L., Prato, S., Brancolini, G., Lovo, M., Torelli, L., 1999. The Eastern Ross Sea continental shelf during the Cenozoic: implications for the West Antarctic ice sheet development. Glob. Planet. Chang. 23 (1), 173–196. https://doi.org/10.1016/S0921-8181(99)00056-9.

De Santis, L., Brancolini, G., Donda, F., 2003. Seismo-stratigraphic analysis of the Wilkes Land continental margin (East Antarctica): influence of glacially driven processes on the Cenozoic deposition. Deep-Sea Res. II Top. Stud. Oceanogr. 50 (8), 1563–1594. https://doi.org/10.1016/S0967-0645(03)00079-1.

De Santis, L., Bergamasco, A., Colizza, E., Geletti, R., Accaino, F., Wardell, N., Olivo, E., Petronio, L., Henrys, S.A., Black, J., Mckay, R.M., Bohm, G., 2015. The Hillary Canyon and the Iselin Bank (Eastern Ross Sea, Antarctica): Alongslope and Downslope Route for Ross Sea Bottom Water. Paper presented at the AGU Fall Meeting Abstracts. https://ui.adsabs.harvard.edu/abs/2015AGUFMEP13A0919D.

DeConto, R.M., Pollard, D., Kowalewski, D., 2012. Reprint of: modeling Antarctic ice sheet and climate variations during Marine Isotope Stage 31. Glob. Planet. Chang. 96-97, 181–188. https://doi.org/10.1016/j.gloplacha.2012.05.018.

Depoorter, M.A., Bamber, J.L., Griggs, J.A., Lenaerts, J.T.M., Ligtenberg, S.R.M., van den Broeke, M.R., Moholdt, G., 2013. Calving fluxes and basal melt rates of Antarctic ice shelves. Nature 502 (7469), 89–92. https://doi.org/10.1038/nature12567.

Domack, E.W., 1990. Laminated terrigenous sediments from the Antarctic Peninsula: the role of subglacial and marine processes. Geol. Soc. Lond., Spec. Publ. 53 (1), 91–103. https://doi.org/10.1144/gsl.Sp.1990.053.01.05.

Donda, F., Brancolini, G., Santis, L.D., Trincardi, F., 2003. Seismic facies and sedimentary processes on the continental rise off Wilkes Land (East Antarctica): evidence of bottom current activity. Deep-Sea Res. II Top. Stud. Oceanogr. 50 (8), 1509–1527. https://doi.org/10.1016/S0967-0645(03)00075-4.

Dowdeswell, J.A., Whittington, R.J., Marienfeld, P., 1994. The origin of massive diamicton facies by iceberg rafting and scouring, Scoresby Sund, East Greenland. Sedimentology 41 (1), 21–35. https://doi.org/10.1111/j.1365-3091.1994.tb01390.x.

Escutia, C., Eittreim, S.L., Cooper, A.K., Nelson, C.H., 2000. Morphology and acoustic character of the Antarctic Wilkes land turbidite systems: ice-sheet-sourced versus river-sourced fans. J. Sediment. Res. 70 (1), 84–93. https://doi.org/10.1306/2DC40900-0E47-11D7-8643000102C1865D.

Escutia, C., Warnke, D., Acton, G.D., Barcena, A., Burckle, L., Canals, M., Frazee, C.S., 2003. Sediment distribution and sedimentary processes across the Antarctic Wilkes Land margin during the Quaternary. Deep-Sea Res. II Top. Stud. Oceanogr. 50 (8), 1481–1508. https://doi.org/10.1016/S0967-0645(03)00073-0.

Escutia, C., De Santis, L., Donda, F., Dunbar, R.B., Cooper, A.K., Brancolini, G., Eittreim, S.L., 2005. Cenozoic ice sheet history from East Antarctic Wilkes Land continental margin sediments. Glob. Planet. Chang. 45 (1), 51–81. https://doi.org/10.1016/j.gloplacha.2004.09.010.

Escutia, C., Brinkhuis, H., Klaus, A., 2011. IODP expedition 318: from greenhouse to icehouse at the Wilkes Land Antarctic Margin. In: Scientific Drilling: Reports on Deep Earth Sampling and Monitoring, 12, pp. 15–23. https://doi.org/10.1016/B978-0-444-62617-2.00012-8.

Fillon, R.H., 1975. Late Cenozoic Paleo-Oceanography of the Ross Sea, Antarctica. GSA Bull. 86 (6), 839–845. https://doi.org/10.1130/0016-7606(1975)86<839:Lcpotr>2.0.Co;2.

Fisher, R.V., 1983. Flow transformations in sediment gravity flows. Geology 11 (5), 273–274. https://doi.org/10.1130/0091-7613(1983)11<273:Ftisgf>2.0.Co;2.

Gales, J.A., Hillenbrand, C.D., Larter, R.D., Laberg, J.S., Melles, M., Benetti, S., Passchier, S., 2018. Processes influencing differences in Arctic and Antarctic trough mouth fan sedimentology. Geological Society, London, Special Publications 475. https://doi.org/10.1144/sp475.7. SP475.477.

Gales, J., Rebesco, M., De Santis, L., Bergamasco, A., Colleoni, F., Kim, S., Accettella, D., Kovacevic, V., Liu, Y., Olivo, E., Colizza, E., Florindo-Lopez, C., Zgur, F., McKay, R., 2021. Role of dense shelf water in the development of Antarctic submarine canyon morphology. Geomorphology 372, 107453. https://doi.org/10.1016/j.geomorph.2020.107453.

Goffart, A., Catalano, G., Hecq, J.H., 2000. Factors controlling the distribution of diatoms and Phaeocystis in the Ross Sea. J. Mar. Syst. 27 (1), 161–175. https://doi.org/10.1016/S0924-7963(00)00065-8.

Gradstein, F.M., Ogg, J.G., Schmitz, M., Ogg, G., 2012. The Geologic Time Scale 2012. Elsevier.

Greenwood, S.L., Gyllencreutz, R., Jakobsson, M., Anderson, J.B., 2012. Ice-flow switching and East/West Antarctic Ice Sheet roles in glaciation of the western Ross Sea. GSA Bull. 124 (11−12), 1736–1749. https://doi.org/10.1130/b30643.1.

Halberstadt, A.R.W., Simkins, L.M., Greenwood, S.L., Anderson, J.B., 2016. Past ice-sheet behaviour: retreat scenarios and changing controls in the Ross Sea, Antarctica. Cryosphere 10 (3), 1003–1020. https://doi.org/10.5194/tc-10-1003-2016.

Halberstadt, A.R.W., Simkins, L.M., Anderson, J.B., Prothro, L.O., Bart, P.J., 2018. Characteristics of the deforming bed: till properties on the deglaciated Antarctic continental shelf. J. Glaciol. 64 (248), 1014–1027. https://doi.org/10.1017/jog.2018.92.

Hampton, M., 1975. Competence of fine-grained debris flows. J. Sediment. Res. 45 (4), 834–844. https://doi.org/10.1306/212f6e5b-2b24-11d7-8648000102c1865d.

Harig, C., Simons, F.J., 2015. Accelerated West Antarctic ice mass loss continues to outpace East Antarctic gains. Earth Planet. Sci. Lett. 415, 134–141. https://doi.org/10.1016/j.epsl.2015.01.029.

Hayes, D.E., Frakes, L.A., Barrett, P.J., Burns, D.A., Chen, P.-H., Ford, A.B., Kaneps, A.G., Kemp, E.M., McCollum, D.W., Piper, D.J.W., Wall, R.E., Webb, P.N., 1973. Sites 270, 271, 272. Retrieved from Texas A & M University, Ocean Drilling Program, College Station, TX, United States.

Hesse, R., Khodabakhsh, S., Klaucke, I., Ryan, W.B.F., 1997. Asymmetrical turbid surface-plume deposition near ice-outlets of the Pleistocene Laurentide ice sheet in the Labrador Sea. Geo-Mar. Lett. 17 (3), 179–187. https://doi.org/10.1007/s003670050024.

Hilgen, F.J., Lourens, L.J., Van Dam, J.A., Beu, A.G., Boyes, A.F., Cooper, R.A., Krijgsman, W., Ogg, J.G., Piller, W.E., Wilson, D.S., 2012. Chapter 29 - the Neogene period. In: Gradstein, F.M., Ogg, J.G., Schmitz, M.D., Ogg, G.M. (Eds.), The Geologic Time Scale. Elsevier, Boston, pp. 923–978.

Hillenbrand, C.D., Ehrmann, W., Larter, R.D., Benetti, S., Dowdeswell, J.A., Cofaigh, Ó., Graham, A.G.C., Grobe, H., 2009a. Clay mineral provenance of sediments in the southern Bellingshausen Sea reveals drainage changes of the West Antarctic Ice Sheet during the Late Quaternary. Mar. Geol. 265 (1), 1–18. https://doi.org/10.1016/j.margeo.2009.06.009.

Hillenbrand, C.D., Kuhn, G., Frederichs, T., 2009b. Record of a Mid-Pleistocene depositional anomaly in West Antarctic continental margin sediments: an indicator for ice-sheet collapse? Quat. Sci. Rev. 28 (13), 1147–1159. https://doi.org/10.1016/j.quascirev.2008.12.010.

Hughes, T., 1973. Is the west Antarctic Ice Sheet disintegrating? Journal of Geophysical Research 78 (33), 7884–7910. https://doi.org/10.1029/JC078i033p07884.

Jacobs, S.S., 1991. On the nature and significance of the Antarctic Slope Front. Mar. Chem. 35 (1–4), 9–24. https://doi.org/10.1016/s0304-4203(09)90005-6.

Jacobs, S.S., Haines, W.E., 1982. Oceanographic Data in the Ross Sea and along George V Coast 1976–1979.

Jacobs, S.S., Amos, A.F., Bruchhausen, P.M., 1970. Ross sea oceanography and antarctic bottom water formation. Deep-Sea Res. Oceanogr. Abstr. 17 (6), 935–962. https://doi.org/10.1016/0011-7471(70)90046-X.

Kennett, J.P., 1968. The fauna of the Ross Sea. Part 6: Ecology and distribution of Foraminifera. In: New Zealand Department of Scientific and Industrial Research Bulletin, 186.

Keys, H., Fowler, D., 1989. Sources and Movement of Icebergs in the South-West Ross Sea, Antarctica. Ann. Glaciol. 12, 85–88. https://doi.org/10.3189/S026030550000700X.

Kim, S., De Santis, L., Hong, J.K., Cottlerle, D., Petronio, L., Colizza, E., Kim, Y.G., Kang, S.G., Kim, H.J., Kim, S., Wardell, N., Geletti, R., Bergamasco, A., McKay, R., Jin, Y.K., Kang, S.H., 2018. Seismic stratigraphy of the Central Basin in northwestern Ross Sea slope and rise, Antarctica: clues to the late Cenozoic ice-sheet dynamics and bottom current activity. Mar. Geol. 395, 363–379. https://doi.org/10.1016/j.margeo.2017.10.013.

King, E.L., Haflidason, H., Sejrup, H.P., Løvlie, R., 1998. Glacigenic debris flows on the North Sea Trough Mouth Fan during ice stream maxima. Mar. Geol. 152 (1), 217–246. https://doi.org/10.1016/S0025-3227(98)00072-3.

Kurtz, D.D., Anderson, J.B., 1979. Recognition and sedimentologic description of recent debris flow deposits from the Ross and Weddell Seas, Antarctica. J. Sediment. Res. 49 (4), 1159–1169. https://doi.org/10.1306/212F78D8-2B24-11D7-8648000102C1865D.

Kuvaas, B., Leitchenkov, G., 1992. Glaciomarine turbidite and current controlled deposits in Prydz Bay, Antarctica. Mar. Geol. 108 (3), 365–381. https://doi.org/10.1016/0025-3227(92)90205-V.

Kuvaas, B., Kristoffersen, Y., Guseva, J., Leitchenkov, G., Gandjukhin, V., Løvås, O., Sand, M., Brekke, H., 2005. Interplay of turbidite and contourite deposition along the Cosmonaut Sea/Enderby Land margin, East Antarctica. Mar. Geol. 217 (1), 143–159. https://doi.org/10.1016/j.margeo.2005.02.025.

Laberg, J.S., Vorren, T.O., 1995. Late Weichselian submarine debris flow deposits on the Bear Island Trough Mouth Fan. Mar. Geol. 127 (1), 45–72. https://doi.org/10.1016/0025-3227(95)00055-4.

Laberg, J.S., Vorren, T.O., 1996. The Middle and Late Pleistocene evolution and the Bear Island Trough Mouth Fan. Glob. Planet. Chang. 12 (1), 309–330. https://doi.org/10.1016/0921-8181(95)00026-7.

Laberg, J.S., Vorren, T.O., 2000. Flow behaviour of the submarine glacigenic debris flows on the Bear Island Trough Mouth Fan, western Barents Sea. Sedimentology 47 (6), 1105–1117. https://doi.org/10.1046/j.1365-3091.2000.00343.x.

Lee, J.I., McKay, R.M., Golledge, N.R., Yoon, H.I., Yoo, K.-C., Kim, H.J., Hong, J.K., 2017. Widespread persistence of expanded East Antarctic glaciers in the southwest Ross Sea during the last deglaciation. Geology 45 (5), 403–406. https://doi.org/10.1130/g38715.1.

Licht, K.J., Dunbar, N.W., Andrews, J.T., Jennings, A.E., 1999. Distinguishing subglacial till and glacial marine diamictons in the western Ross Sea, Antarctica: implications for a last glacial maximum grounding line. GSA Bull. 111 (1), 91–103 doi:10.1130/0016-7606(1999)111<0091:Dstagm>2.3.Co;2.

Lindeque, A., Gohl, K., Henrys, S., Wobbe, F., Davy, B., 2016. Seismic stratigraphy along the Amundsen Sea to Ross Sea continental rise: a cross-regional record of pre-glacial to glacial processes of the West Antarctic margin. Palaeogeogr. Palaeoclimatol. Palaeoecol. 443, 183–202. https://doi.org/10.1016/j.palaeo.2015.11.017.

Lisiecki, L.E., Raymo, M.E., 2005. A Pliocene-Pleistocene stack of 57 globally distributed benthic δ18O records. Paleoceanography 20 (1). https://doi.org/10.1029/2004PA001071.

Lourens, L., Hilgen, F., Shackleton, N.J., Laskar, J., Wilson, D., 2004. The Neogene period. In: Gradstein, F.M., Ogg, J.G., Smith, A. (Eds.), A Geologic Time Scale (2004). Cambridge University Press, Cambridge, United Kingdom, pp. 409–440.

Lowe, D.R., 1982. Sediment gravity flows; II, Depositional models with special reference to the deposits of high-density turbidity currents. J. Sediment. Res. 52 (1), 279–297. https://doi.org/10.1306/212F7F31-2B24-11D7-8648000102C1865D.

Lucchi, R.G., Rebesco, M., 2007. Glacial contourites on the Antarctic Peninsula margin: insight for palaeoenvironmental and palaeoclimatic conditions. Geol. Soc. Lond., Spec. Publ. 276 (1), 111–127. https://doi.org/10.1144/GSL.SP.2007.276.01.06.

Lucchi, R.G., Rebesco, M., Camerlenghi, A., Busetti, M., Tomadin, L., Villa, G., Persico, D., Morigi, C., Bonci, M.C., Giorgetti, G., 2002. Mid-late Pleistocene glacimarine sedimentary processes of a high-latitude, deep-sea sediment drift (Antarctic Peninsula Pacific margin). Mar. Geol. 189 (3–4), 343–370. https://doi.org/10.1016/S0025-3227(02)00470-X.

Lucchi, R.G., Camerlenghi, A., Rebesco, M., Colmenero-Hidalgo, E., Sierro, F.J., Sagnotti, L., Urgeles, R., Melis, R., Morigi, C., Bárcena, M.A., Giorgetti, G., Villa, G., Persico, D., Flores, J.A., Rigual-Hernández, A.S., Pedrosa, M.T., Macri, P., Caburlotto, A., 2013. Postglacial sedimentary processes on the Storfjorden and Kveithola trough mouth fans: significance of extreme glacimarine sedimentation.

Glob. Planet. Chang. 111, 309–326. https://doi.org/10.1016/j.gloplacha.2013.10.008.
Majewski, W., Bart, P.J., McGlannan, A.J., 2018. Foraminiferal assemblages from ice-proximal paleo-settings in the Whales Deep Basin, eastern Ross Sea, Antarctica. Palaeogeogr. Palaeoclimatol. Palaeoecol. 493, 64–81. https://doi.org/10.1016/j.palaeo.2017.12.041.
McKay, R.M., Browne, G., Carter, L., Cowan, E.A., Dunbar, G., Krissek, L., Naish, T., Powell, R.D., Reed, J., Talarico, F.M., Wilch, T., 2009. The stratigraphic signature of the late Cenozoic Antarctic Ice Sheets in the Ross Embayment. Geol. Soc. Am. Bull. 121 (11–12), 1537–1561. https://doi.org/10.1130/b26540.1.
McKay, R., Bendle, J., Cook, C., Dunbar, G., Dunbar, R.B., Escutia, C., González, J.J., Jiménez, F., Naish, T., Passchier, S., Riesselman, C.R., Scherer, R.P., Tauxe, L., Toney, J.L., van de Flierdt, T., Welsh, K.J., Scientists, I.E.S., 2011. Early to Mid-Pleistocene Warm Events at the Antarctic Margin. https://ui.adsabs.harvard.edu/abs/2011AGUFMPP44A..08M.
McKay, R.M., Naish, T., Powell, R.D., Barrett, P., Scherer, R.P., Talarico, F.M., Kyle, P., Monien, D., Kuhn, G., Jackolski, C., Williams, T., 2012. Pleistocene variability of Antarctic Ice Sheet extent in the Ross Embayment. Quat. Sci. Rev. 34, 93–112. https://doi.org/10.1016/j.quascirev.2011.12.012.
McKay, R.M., De Santis, L., Kulhanek, D.K., Ash, J.L., Beny, F., Browne, I.M., Cortese, G., Cordeiro de Sousa, I.M., Dodd, J.P., Esper, O.M., Gales, J.A., Harwood, D.M., Ishino, S., Keisling, B.A., Kim, S., Kim, S., Laberg, J.S., Leckie, R.M., Müller, J., Patterson, M.O., Romans, B.W., Romero, O.E., Sangiorgi, F., Seki, O., Shevenell, A.E., Singh, S.M., Sugisaki, S.T., van de Flierdt, T., van Peer, T.E., Xiao, W., Xiong, Z., the Expedition 374 Scientists, 2019a. Expedition 374 methods. In: Proceedings of the International Ocean Discovery Program, 374: College Station, TX (International Ocean Discovery Program). https://doi.org/10.14379/iodp.proc.374.102.2019.
McKay, R.M., De Santis, L., Kulhanek, D.K., Ash, J.L., Beny, F., Browne, I.M., Cortese, G., Cordeiro de Sousa, I.M., Dodd, J.P., Esper, O.M., Gales, J.A., Harwood, D.M., Ishino, S., Keisling, B.A., Kim, S., Kim, S., Laberg, J.S., Leckie, R.M., Müller, J., Patterson, M.O., Romans, B.W., Romero, O.E., Sangiorgi, F., Seki, O., Shevenell, A.E., Singh, S.M., Sugisaki, S.T., van de Flierdt, T., van Peer, T.E., Xiao, W., Xiong, Z., the Expedition 374 Scientists, 2019b. Site U1525. In: Proceedings of the International Ocean Discovery Program, 374: College Station, TX (International Ocean Discovery Program). https://doi.org/10.14379/iodp.proc.374.107.2019.
McMillan, M., Shepherd, A., Sundal, A., Briggs, K., Muir, A., Ridout, A., Hogg, A., Wingham, D., 2014. Increased ice losses from Antarctica detected by CryoSat-2. Geophysical Research Letters 41 (11), 3899–3905. https://doi.org/10.1002/2014GL060111.
Melles, M., 1991. Paläoglaziologie und Paläozeanographie im Spätquartär am Kontinentalrand des südlichen Weddellmeeres. University of Bremen, Antarktis.
Michels, K.H., Rogenhagen, J., Kuhn, G., 2001. Recognition of contour-current influence in mixed contourite-turbidite sequences of the western Weddell Sea, Antarctica. Mar. Geophys. Res. 22 (5–6), 465–485. https://doi.org/10.1023/A:1016303817273.
Miramontes, E., Eggenhuisen, J.T., Jacinto, R.S., Poneti, G., Pohl, F., Normandeau, A., Campbell, D.C., Hernández-Molina, F.J., 2020. Channel-levee evolution in combined contour current–turbidity current flows from flume-tank experiments. Geology 48 (4), 353–357. https://doi.org/10.1130/g47111.1.
Morrison, A.K., Hogg, A.M., England, M.H., Spence, P., 2020. Warm Circumpolar Deep Water transport toward Antarctica driven by local dense water export in canyons. Science Advances 6 (18), eaav2516. https://doi.org/10.1126/sciadv.aav2516.
Mosola, A.B., Anderson, J.B., 2006. Expansion and rapid retreat of the West Antarctic Ice Sheet in eastern Ross Sea: possible consequence of over-extended ice streams? Quat. Sci. Rev. 25 (17–18), 2177–2196. https://doi.org/10.1016/j.quascirev.2005.12.013.
Mulder, T., Berry, J.A., Piper, D.J.W., 1997. Links between morphology and geotechnical characteristics of large debris flow deposits in the Albatross Area on the Scotian Slope (SE Canada). Marine Georesources & Geotechnology 15 (3), 253–281. https://doi.org/10.1080/10641199709379947.
Mulder, T., Faugères, J.C., Gonthier, E., 2008. Chapter 21 Mixed turbidite–contourite systems. In: Rebesco, M., Camerlenghi, A. (Eds.), Developments in Sedimentology, 60. Elsevier, pp. 435–456.
Naish, T., Powell, R., Levy, R., Wilson, G., Scherer, R., Talarico, F., Krissek, L., Niessen, F., Pompilio, M., Wilson, T., 2009. Obliquity-paced Pliocene West Antarctic ice sheet oscillations. Nature 458 (7236), 322.
Noormets, R., Dowdeswell, J.A., Larter, R.D., Cofaigh, Ó., C., & Evans, J., 2009. Morphology of the upper continental slope in the Bellingshausen and Amundsen Seas – implications for sedimentary processes at the shelf edge of West Antarctica. Mar. Geol. 258 (1), 100–114. https://doi.org/10.1016/j.margeo.2008.11.011.
Ó Cofaigh, C., Taylor, J., Dowdeswell, J.A., Pudsey, C.J., 2003. Palaeo-ice streams, trough mouth fans and high-latitude continental slope sedimentation. Boreas 32 (1), 37–55. https://doi.org/10.1080/03009480310001858.
Orsi, A.H., Wiederwohl, C.L., 2009. A recount of Ross Sea waters. Deep-Sea Res. II Top. Stud. Oceanogr. 56 (13–14), 778–795. https://doi.org/10.1016/j.dsr2.2008.10.033.
Passchier, S., O'Brien, P.E., Damuth, J.E., Januszczak, N., Handwerger, D.A., Whitehead, J.M., 2003. Pliocene–Pleistocene glaciomarine sedimentation in eastern Prydz Bay and development of the Prydz trough-mouth fan, ODP Sites 1166 and 1167, East Antarctica. Mar. Geol. 199 (3), 279–305. https://doi.org/10.1016/S0025-3227(03)00160-9.
Passchier, S., Browne, G., Field, B., Fielding, C.R., Krissek, L.A., Panter, K., Pekar, S.F., Team, a. A.-S. S, 2011. Early and middle Miocene Antarctic glacial history from the sedimentary facies distribution in the AND-2A drill hole, Ross Sea, Antarctica. GSA Bull. 123 (11–12), 2352–2365. https://doi.org/10.1130/b30334.1.
Patterson, M.O., McKay, R., Naish, T., Escutia, C., Jimenez-Espejo, F.J., Raymo, M.E., Meyers, S.R., Tauxe, L., Brinkhuis, H., Klaus, A., Fehr, A., Bendle, J.A.P., Bijl, P.K., Bohaty, S.M., Carr, S.A., Dunbar, R.B., Flores, J.A., Gonzalez, J.J., Hayden, T.G., Iwai, M., Katsuki, K., Kong, G.S., Nakai, M., Olney, M.P., Passchier, S., Pekar, S.F., Pross, J., Riesselman, C.R., Röhl, U., Sakai, T., Shrivastava, P.K., Stickley, C.E., Sugasaki, S., Tuo, S., van de Flierdt, T., Welsh, K., Williams, T., Yamane, M., Scientists, I.E., 2014. Orbital forcing of the East Antarctic ice sheet during the Pliocene and Early Pleistocene. Nat. Geosci. 7 (11), 841–847. https://doi.org/10.1038/ngeo2273.
Peakall, J., McCaffrey, B., Kneller, B., 2000. A process model for the evolution, morphology, and architecture of sinuous submarine channels. Journal of Sedimentary Research 70, 434–448. https://doi.org/10.1306/2DC4091C-0E47-11D7-8643000102C1865D.
Perotti, M., Andreucci, B., Talarico, F., Zattin, M., Langone, A., 2017. Multianalytical provenance analysis of Eastern Ross Sea LGM till sediments (Antarctica): petrography, geochronology, and thermochronology detrital data. Geochem. Geophys. Geosyst. 18 (6), 2275–2304. https://doi.org/10.1002/2016GC006728.
Piper, D.J.W., Brisco, C.D., 1975. Deep-water continental margin sedimentation, DSDP, Leg 28, Antarctica. Initial Rep. Deep Sea Drill. Proj. 28, 727–755. https://doi.org/10.2973/dsdp.proc.28.121.1975.
Piper, D.J.W., Normark, W.R., 1983. Turbidite depositional patterns and flow characteristics, Navy Submarine Fan, California Borderland. Sedimentology 30 (5), 681–694. https://doi.org/10.1111/j.1365-3091.1983.tb00702.x.
Pollard, D., DeConto, R.M., 2009. Modelling West Antarctic ice sheet growth and collapse through the past five million years. Nature 458, 329. https://doi.org/10.1038/nature07809.
Prothro, L.O., Simkins, L.M., Majewski, W., Anderson, J.B., 2018. Glacial retreat patterns and processes determined from integrated sedimentology and geomorphology records. Mar. Geol. 395, 104–119. https://doi.org/10.1016/j.margeo.2017.09.012.
Pudsey, C.J., 2000. Sedimentation on the continental rise west of the Antarctic Peninsula over the last three glacial cycles. Mar. Geol. 167 (3), 313–338. https://doi.org/10.1016/S0025-3227(00)00039-6.
Pudsey, C.J., 2002. Neogene Record of Antarctic Peninsula Glaciation in Continental Rise Sediments: ODP Leg 178, Site 1095. Proceedings of the Ocean Drilling Program: Scientific Results, 178, pp. 1–25. https://doi.org/10.2973/odp.proc.sr.178.214.2001.
Pudsey, C.J., Camerlenghi, A., 1998. Glacial–interglacial deposition on a sediment drift on the Pacific margin of the Antarctic Peninsula. Antarct. Sci. 10 (3), 286–308. https://doi.org/10.1017/S0954102098000376.
Rebesco, M., Camerlenghi, A., Geletti, R., Canals, M., 2006. Margin architecture reveals the transition to the modern Antarctic ice sheet ca. 3 Ma. Geology 34 (4), 301–304. https://doi.org/10.1130/g22000.1.
Rebesco, M., Camerlenghi, A., Volpi, V., Neagu, C., Accettella, D., Lindberg, B., Cova, A., Zgur, F., 2007. Interaction of processes and importance of contourites: insights from the detailed morphology of sediment Drift 7, Antarctica. Geol. Soc. Lond., Spec. Publ. 276 (1), 95–110. https://doi.org/10.1144/gsl.Sp.2007.276.01.05.
Rebesco, M., Hernandez-Molina, F.J., Van Rooij, D., Wahlin, A., 2014. Contourites and associated sediments controlled by deep-water circulation processes: state-of-the-art and future considerations. Mar. Geol. 352, 111–154. https://doi.org/10.1016/j.margeo.2014.03.011.
Rignot, E., Mouginot, J., Scheuchl, B., van den Broeke, M., van Wessem, M.J., Morlighem, M., 2019. Four decades of Antarctic Ice Sheet mass balance from 1979–2017. Proc. Natl. Acad. Sci. 116 (4), 1095–1103. https://doi.org/10.1073/pnas.1812883116.
Salles, T., Marchès, E., Dyt, C., Griffiths, C., Hanquiez, V., Mulder, T., 2010. Simulation of the interactions between gravity processes and contour currents on the Algarve Margin (South Portugal) using the stratigraphic forward model Sedsim. Sediment. Geol. 229 (3), 95–109. https://doi.org/10.1016/j.sedgeo.2009.05.007.
Scherer, R.P., Bohaty, S.M., Dunbar, R.B., Esper, O., Flores, J.-A., Gersonde, R., Harwood, D.M., Roberts, A.P., Taviani, M., 2008. Antarctic records of precession-paced insolation-driven warming during early Pleistocene Marine Isotope Stage 31. Geophys. Res. Lett. 35 (3) https://doi.org/10.1029/2007gl032254.
Schröder, L., Horwath, M., Dietrich, R., Helm, V., van den Broeke, M.R., Ligtenberg, S.R.M., 2019. Four decades of Antarctic surface elevation changes from multi-mission satellite altimetry. Cryosphere 13 (2), 427–449. https://doi.org/10.5194/tc-13-427-2019.
Shanmugam, G., 1997. The Bouma Sequence and the turbidite mind set. Earth Sci. Rev. 42 (4), 201–229. https://doi.org/10.1016/S0012-8252(97)81858-2.
Shepherd, A., Ivins, E., Rignot, E., Smith, B., van den Broeke, M., Velicogna, I., Whitehouse, P., Briggs, K., Joughin, I., Krinner, G., 2018. Mass balance of the Antarctic Ice Sheet from 1992 to 2017. Nature 556, 219–222. https://doi.org/10.1038/s41586-018-0179-y.
Shipp, S., Anderson, J., Domack, E., 1999. Late Pleistocene–Holocene retreat of the West Antarctic Ice-Sheet system in the Ross Sea: Part 1—Geophysical results. GSA Bull. 111 (10), 1486–1516 doi:10.1130/0016-7606(1999)111<1486:Lphrot>2.3.Co;2.
Sinclair, H.D., Tomasso, M., 2002. Depositional evolution of confined turbidite basins. J. Sediment. Res. 72 (4), 451–456. https://doi.org/10.1306/111501720451.
Smith, J.A., Graham, A.G.C., Post, A.L., Hillenbrand, C.-D., Bart, P.J., Powell, R.D., 2019. The marine geological imprint of Antarctic ice shelves. Nat. Commun. 10 (1), 5635. https://doi.org/10.1038/s41467-019-13496-5.
Stein, K., Timmermann, A., Kwon, E.Y., Friedrich, T., 2020. Timing and magnitude of Southern Ocean sea ice/carbon cycle feedbacks. Proc. Natl. Acad. Sci. 117 (9), 4498. https://doi.org/10.1073/pnas.1908670117.
Stow, D.A.V., 1985. Fine-grained sediments in deep water: an overview of processes and facies models. Geo-Mar. Lett. 5 (1), 17–23. https://doi.org/10.1007/BF02629792.
Stow, D.A.V., Piper, D.J.W., 1984. Deep-water fine-grained sediments: facies models. Geol. Soc. Lond., Spec. Publ. 15 (1), 611–646. https://doi.org/10.1144/gsl.Sp.1984.015.01.38.

Stow, D.A.V., Smillie, Z., 2020. Distinguishing between deep-water sediment facies: turbidites, contourites and hemipelagites. Geosciences 10, 68. https://doi.org/10.3390/geosciences10020068.

Stow, D.A.V., Faugères, J.-C., Howe, J.A., Pudsey, C.J., Viana, A.R., 2002. Bottom currents, contourites and deep-sea sediment drifts: current state-of-the-art. Geological Society, London, Memoirs 22 (1), 7. https://doi.org/10.1144/GSL.MEM.2002.022.01.02.

Teitler, L., Florindo, F., Warnke, D.A., Filippelli, G.M., Kupp, G., Taylor, B., 2015. Antarctic Ice Sheet response to a long warm interval across Marine Isotope Stage 31: a cross-latitudinal study of iceberg-rafted debris. Earth Planet. Sci. Lett. 409, 109–119. https://doi.org/10.1016/j.epsl.2014.10.037.

Tripsanas, E.K., Piper, D.J.W., 2008. Glaciogenic debris-flow deposits of Orphan Basin, offshore eastern Canada: sedimentological and rheological properties, origin, and relationship to meltwater discharge. J. Sediment. Res. 78 (11), 724–744. https://doi.org/10.2110/jsr.2008.082.

Tziperman, E., Gildor, H., 2003. On the mid-Pleistocene transition to 100-kyr glacial cycles and the asymmetry between glaciation and deglaciation times. Paleoceanography 18 (1). https://doi.org/10.1029/2001pa000627, 1-1-1-8.

Villa, G., Lupi, C., Cobianchi, M., Florindo, F., Pekar, S.F., 2008. A Pleistocene warming event at 1 Ma in Prydz Bay, East Antarctica: evidence from ODP Site 1165. Palaeogeogr. Palaeoclimatol. Palaeoecol. 260 (1), 230–244. https://doi.org/10.1016/j.palaeo.2007.08.017.

Villa, G., Persico, D., Wise, S.W., Gadaleta, A., 2012. Calcareous nannofossil evidence for Marine Isotope Stage 31 (1Ma) in Core AND-1B, ANDRILL McMurdo Ice Shelf Project (Antarctica). Glob. Planet. Chang. 96-97, 75–86. https://doi.org/10.1016/j.gloplacha.2009.12.003.

Vorren, T.O., Laberg, J.S., 1997. Trough mouth fans — palaeoclimate and ice-sheet monitors. Quat. Sci. Rev. 16 (8), 865–881. https://doi.org/10.1016/S0277-3791(97)00003-6.

Wang, D., Hesse, R., 1996. Continental slope sedimentation adjacent to an ice-margin. II. Glaciomarine depositional facies on labrador slope and glacial cycles. Marine Geology 135 (1), 65–96. https://doi.org/10.1016/S0025-3227(96)00012-6.

Weertman, J., 1974. Stability of the junction of an ice sheet and an ice shelf. Journal of Glaciology 13 (67), 3–11. https://doi.org/10.3189/S0022143000023327.

Wei, J.H., Finkelstein, D.B., Brigham-Grette, J., Castañeda, I.S., Nowaczyk, N., 2014. Sediment colour reflectance spectroscopy as a proxy for wet/dry cycles at Lake El'gygytgyn, Far East Russia, during Marine Isotope Stages 8 to 12. Sedimentology 61 (6), 1793–1811. https://doi.org/10.1111/sed.12116.

Whitworth, T., Orsi, A.H., 2006. Antarctic Bottom Water production and export by tides in the Ross Sea. Geophys. Res. Lett. 33 (12) https://doi.org/10.1029/2006GL026357.

Yu, B., Ma, Y., Qi, X., 2013. Experimental study on the influence of clay minerals on the yield stress of debris flows. J. Hydraul. Eng. 139 (4), 364–373. https://doi.org/10.1061/(ASCE)HY.1943-7900.0000679.